Flame Self-Interactions in Turbulent Boundary Layer Flashback of Premixed Hydrogen-Rich Combustion

MEC3029 Final Project

Presented to the
School of Engineering
at
Newcastle University

In Partial Fulfilment of the
Requirements of the Degree

Mechanical Engineering

Author: Mr David Andrew Stewart.
Supervisor: Dr Umair Ahmed
Date: 10/05/2021

Abstract

A three-dimensional Direct Numerical Simulation (DNS) database of a premixed hydrogen-rich flame in turbulent boundary layer flashback has been considered to investigate the distribution of flame topologies associated with flame self-interaction (FSI) events, to the best of the authors' knowledge, for the first time. The analysis has been carried out at different wall normal distances within the channel flow to demonstrate the wall boundary's influence on the statistics of FSIs. It has been found that the presence of the wall boundary has a significant influence on the geometry of the turbulent flames surface, and consequently the overall turbulent burning rate. At all wall normal distances, the FSI events were located within a very confined region at the trailing edge of the flame brush towards the burnt products. Tunnel Formations and Burnt Gas Pockets were prevalent at all distances from the wall followed by Tunnel Closure events. Unburnt Gas Pockets were the rarest flame topology, existing in relatively low numbers towards the middle of the channel flow where the flow velocity is at a maximum. The overall frequency of the FSI events increased as progression is made away from the wall boundary, then subsequently decreases approaching the region at the middle of the channel flow. The results presented in this study have important implications from a modelling perspective where the flame topologies have a strong influence on the geometry of the flames surface, which will inevitably affect and possibly provide an extension to the flame surface-based modelling approaches. Accordingly, the findings of the current analysis might need to be considered when extending such flame surfaced-based models in the context of turbulent premixed flames in boundary layer flashback.

Table of Contents

Declaration

This report is submitted as part of the requirements for the Degree of Mechanical Engineering at the University of Newcastle upon Tyne and has not been submitted for any other degree at this or any other University.

It is solely the work of David Andrew Stewart except were acknowledged in the text or the Acknowledgements below. It describes work carried out at the University of Newcastle upon Tyne which is entirely recorded in a Project Logbook which has been made available for examination.

I am aware of the penalties for plagiarism, fabrication and unacknowledged syndication and declare that this report is free of these.

Authors Signature: 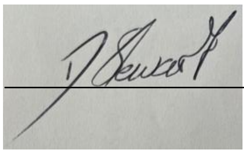 **Date**:12/05/2021

Acknowledgements

I gratefully acknowledge the help in producing this paper from Dr Umair Ahmed. Without his continued support from the onset of the project providing knowledge and resources throughout, this paper would not have been produced. I also gratefully acknowledged the computational support of ROCKET-HPC.

1. Introduction

1.1. Motivation

Climate change is becoming an increasing issue globally, with power generation and civil aviation industries striving to gain a control over pollutant emissions to reduce greenhouse gases. Hydrogen-rich syngas fuels are being considered as a clean and efficient fuel for future large scale power generation and aviation thrust propulsion systems[1]. Hydrogen combustion offers a lower environmental impact having the cleanest combustion pollutants and an infinite hydrogen water cycle[61]. It has a higher energy efficiency[2] relative to conventional combustion fuels such as kerosine and natural gas. This is due to hydrogens burning stability across a range of fuel concentrations during combustion and its relatively easy ignition because of a high flammability range and high burning velocity. However, the aforementioned characteristics of hydrogen lead the increased risk of flashback, which is the uncontrolled transient upstream propagation of a flame[5], and therefor make the development of hydrogen combustors much more challenging[2]. Hydrogen flames introduce further complications with their interactions at boundary layers formed near combustor walls.

The design of modern combustion equipment orientates around flame wall-interaction (FWI) and it is essential to achieve improvements of the predictive capabilities in the modelling of boundary layer flashback[11] for premixed turbulent flames as new combustors are being made smaller to maximise energy density and minimise weight, and the turbulent premixed flame is the utter most common flame mode in such combustors[60]. Whilst boundary layer flashback doesn't pose as a concerning issue in natural gas fuelled gas turbines, evidence suggests that premixed combustion of hydrogen-rich syngas under gas turbine conditions (high reactant temperature, high pressure) presents boundary layer flashback as a significant problem[2,5]. The more reactive nature of hydrogen-rich syngas increases the complexity of boundary layer flashback considerably. When compared with hydrocarbon-air flames, hydrogen-air premixed flames are able to propagate three times (in relation to flame thickness) closer to the wall before heat loss to the solid surface leads to flame quenching,[5] thus adding to the complexity of the physical and chemical phenomena[6,7] associated with FWI. This lower quenching distance of hydrogen-air flames relative to their methane-air counterpart suggests that they can propagate closer to the wall in regions of the boundary layer characterised by very low flow velocities. This also leads to increased heat transfer, which can potentially damage the combustor walls resulting in failure of the combustion equipment. A common way to eliminate the flashback of hydrocarbon flames in conventionally fuelled combustors is to flush the pre-mixer and combustor walls with primary combustion air[5]. However, with hydrogen-rich fuelled gas turbines this method is no longer feasible as all the available air injected is needed for dilution of the highly reactive fuel.

Current modelling approaches used to simulate industrial scale combustion rely on Reynolds Averaged Navier Stokes (RANS) or Large Eddie Simulation (LES) techniques, and they fail to accurately account for the aforementioned physical phenomena involved with turbulent boundary layer flashback.

1.2. Turbulent Premixed Combustion Modelling

Turbulent premixed flames are often comprised of a thin and highly wrinkled layer of reacting gas that forms an interface between extended regions of unburned reactants and hotter, less dense products[21]. The interaction of a flame with a turbulent flow field results in wrinkling of the flame, causing an increase in the flames surface area, subsequently increasing the flames rate of burning. When a flame is subject to high levels of turbulence and flame wrinkling is very pronounced, the flames surface interacts with itself generating local topologies. These topologies (as a result of flame self-interactions) can affect the burning characteristics of such flames significantly through events such as flame pinch off. Flame pinch-off is associated with the formation of an isolated reactant pocket which causes rapid changes in the flames surface area and consequently its burning rate[21].

When considering turbulent premixed combustion, the gradient of a scalar field is used to close the unclosed mean/filtered reaction rate in the context of RANS and LES and relies on the generalized Flame Surface Density (FSD)[8] or Scalar Dissipation Rate (SDR)[9] for modelling. In the present study, the scalar field of choice is the reaction progress variable (RPV) c based of the mass fraction of water vapor Y_{H_2O}. Therefore, it is of fundamental importance to have a comprehensive understanding of the statistical behaviour of the modulus of the RPV gradient $|\nabla c|$, often referred to as the Surface Density Function (SDF), if turbulent premixed combustion is to be modelled with sufficient accuracy[10]. This study will determine the topological structures associated with the scalar field in turbulence based upon the sign of the eigenvalues of the Hessian tensor of the RPV $\underline{\underline{H}}(c)$. The tile-like and flat topologies discussed in this study have appeared to be the dominant topologies for non-reacting mixing[12] and in turbulent premixed flames[13,14]. Many papers express the pivotal role the local flame topology has on characterising flame-flame interactions in turbulent premixed combustion[15-22]. Flame-flame interactions can be analysed in a number of ways, including: Minkowski functional techniques[18,19], automatic feature extraction techniques obtained using complex wavelet transform methods[15,59] and critical point theory[17,20,21], with the latter being applied in this study. There has been considerable analysis of flame-flame interactions in turbulent premixed combustion, however limited effort has been dedicated to such phenomena involved in boundary layer flashback of premixed hydrogen-rich combustion within a turbulent channel. To the best of my knowledge, a detailed analysis of the topological nature of flame self-interactions (FSI) in premixed combustion of a hydrogen-rich flame at the boundary layer and throughout during boundary layer flashback, present within a turbulent shear induced flow field, is yet to be carried out in the existing literature publicly available. Detailed models of reacting and non-reacting combustion within turbulent flows can be accurately simulated using Direct Numerical Simulation (DNS) techniques and has proved an invaluable source to gain a fundamental understanding of the phenomena involved in each[23-26]. To fill the aforementioned gaps in the existing literature, a DNS database for boundary layer flashback of a premixed hydrogen-air flame with equivalence ratio 1.5 in a fully developed turbulent channel flow has been interrogated for analysis. This database has been analysed in several previous studies to investigate the effects of pressure oscillations[27] and turbulent kinetic energy transport physics[3] during turbulent boundary layer flashback, but none of the aforementioned analysis focused on the local topologies associated with flame-self interactions during boundary layer flashback. Achieving a comprehensive understanding of the previously mentioned statistics related to the surface density function is necessary for improving the FSD[8] and SDR[9] models.

1.3. Aims and Objectives

The main aims and objectives of this present study are as follows:

- To interrogate a DNS dataset corresponding to a premixed hydrogen-air flame with equivalence ratio of 1.5 in turbulent boundary layer flashback at different distances from the wall boundary to identify the predominant topological geometries and their distribution associated with flame self-interactions (FSIs).
- To carry out a statistical analysis involving the principal curvatures of a premixed hydrogen-air flame with an equivalence ratio of 1.5 in turbulent boundary layer flashback to gain a fundamental insight into the physical processes associated to the formulation of the identified FSI topologies and investigate the influence of the boundary layer wall on the FSIs.

The rest of the report is organised as follows. Section 2 describes the DNS dataset used and its configuration, section 3 outlines the relevant mathematical background and numerical implementation. This is followed by a presentation of the results obtained and a discussion seen in section 4, finalised by any conclusions summarised in section 5.

2. DNS Datasets and Configuration

The same DNS dataset for boundary layer flashback as performed in the earlier work of Kitano *et al*[27] has been analysed in this current study. The configuration of the flow, the turbulence flow field, and the flames characteristics are all similar to those within the earlier study carried out by Gruber et al[5]. The DNS database represents a hydrogen-air flame undergoing boundary layer flashback in a channel flow at bulk Reynolds number $Re_b = \rho u_b 2h/\mu = 3500$, with h being the channels half height and $u_b = 1/2h\int_0^{2h} u\, dy = 19.83 m/s$. The Reynolds number is based on the channel half height h and the friction velocity $Re_\tau = \rho u_\tau h/\mu = 120$ with $u_\tau = \sqrt{|\tau_w|/\rho}$ and $\tau_w = \mu \partial u/\partial y\,|_{y=0 \text{ or } y=2h}$ being the friction velocity and the wall shear stress respectively. A code knows at FK[3] was used to execute the simulation which has seen previous use in several studies involving turbulent, reacting and multiphase flows[28-32]. FK[3] used finite volume methodologies to solve the conservation equations for mass, momentum, enthalpy and chemical species. A skeletal chemical mechanism is used to account for the chemistry involves in hydrogen-air combustion which comprises of nine chemical species (N_2, H_2, O_2, OH, H_2O, H, O, HO_2, H_2O_2) and twenty reactions, originally being designed for the modelling nitrogen combustion[33]. A fourth-ordered centered scheme is used to solve the spatial derivatives for the momentum equation. A third-ordered quadratic upstream interpolation for convective kinematics (QUICK)[34] scheme is used to evaluate the convective terms of enthalpy and species mass fraction. The remaining terms in the scalar transport equations are calculated using a second-ordered scheme. Many numerical investigations use this method to solve scalar equations involving heat transfer in wall bounded flows to ensure the numerical stability and integrity of the code[35,36]. *Moureau et al*[37] proposed a pressure-based semi-implicit algorithm that is used to accurately solve compressible flow equations associated with hydrogen combustion. Within this fractional-step method, time advancement for the convective terms is executed through a third-order explicit total variation diminishing (TVD) Runge-Kutta method. The chemical kinetics are solved and integrated using a multi-timescale (MTS) method with a minimum time resolution of 1 x 10^{-9} seconds. The multicomponent diffusion for all nine chemical species is solved via the diffusion velocities by

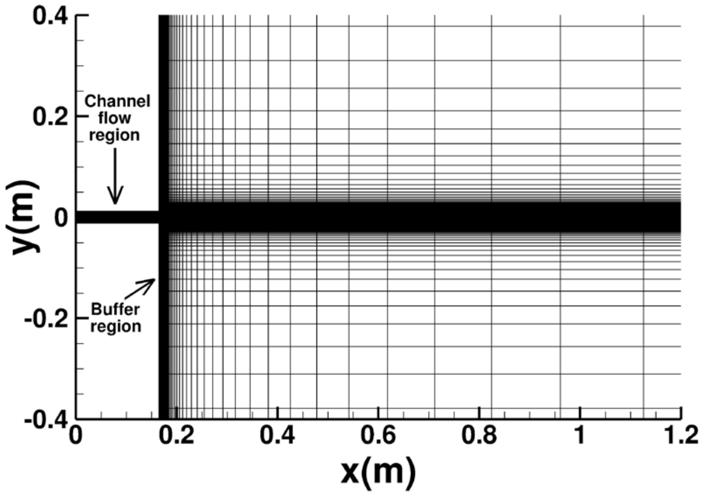

Figure 1. Computational grid used for Direct Numerical Simulation a shown in the x-y mid- plane[3,27,41]

solving a system of linear equations outlines in reference 38 and 39 for every individual grid point at all time steps in the x, y and z directions. CHEMKIN[40] is an efficient FORTRAN code that provides all the binary diffusion coefficients necessary for the diffusion calculations governing the physics of gaseous phase kinetics. The reader is directed to the previous work of Kitano *et al*[27] for a more comprehensive explanation of the numerical techniques applied in this simulation.

The computational domain for the DNS is partitioned into two primary regions, namely, the channel flow region and the buffer region[3,41], as shown in figure 1. The channel flow region is further sub-divided into two parts, being the turbulence generation region and the flashback region, as showing in figure 2[27]. The dimensions of the channel flow region are 173mm x 20mm x 30mm, of which 103mm x 20mm x 30mm consists of the flashback region[27]. Fully developed wall-bounded turbulent flow is generated by imposing a pressure drop and a periodic boundary condition in the x direction within the turbulence generation region of the computational domain. Readers are directed to reference 3 for further detail on how the non-reacting turbulence is introduced into the region of flashback within the channel flow. The outflow characteristics of the upstream channel are introduced to the flashback region of the channel, and after 100ms of the flow becoming fully turbulent, a freely propagating planar flame is initialized in the flashback region of the domain. The walls in the y direction have a no-slip isothermal boundary condition at 750K applied to them, and the walls in the z direction are treated as periodic. The outflow boundaries in the buffer region have the Navier-Stokes Characteristic Boundary Condition (NSCBC)[42] applied to then, as shown in figure 1.

The parameters for the initial gas temperature, pressure, and equivalence ratio are given a value of 750K, 0.1MPa and 1.5 respectively[3,27,41]. The laminar burning velocity S_L and the flames thermal thickness $\delta_{th} = (T_{ad} - T_R)/max|\nabla T|_L$ (with T_R being the reactant temperature, T_{ad} being the adiabatic flame temperature, and the subscript L representing the laminar flame quantities). Under the aforementioned conditions, S_L and δ_{th} are determined to be 14m/s and 0.48mm respectively[43]. The resolution of the grid in the flashback region of the simulation is 50 μm, and in non-dimensional wall units equates to $\Delta x^+ = \Delta y^+ = \Delta z^+ = 0.6$. The resolution of the grid points within the simulation is sufficient as it guarantees that the laminar flame thermal thickness δ_{th} is resolved in approximately 10 grid points. This criterion also satisfies the resolution criteria as recommended by Moser *et al*[44] for turbulent boundary layer combustion up to a Reynolds shear stress of 590. Within the turbulence generation region of the computational domain, a larger grid spacing of 700 μm (Δx^+=0.84) is used in the x-direction which is sufficient for this body of work to resolve the non-reacting turbulence at the aforementioned conditions. In total, approximately 0.4 billion grid points are used within the simulation, 1150 x 400 x 600 (276 million) of which are situated within the flashback region of the domain.

A sample is taken from the data 1.6 ms after the freely propagating planar flame is initialised in the flashback region of the domain which ensures a steady flashback speed has been attained. The earlier study by Kitano *et al*[27] provides more detail on this. Freely propagating statistically planner turbulent premixed flames[8,45] and laboratory scale jet flame[46-48] have been analysed using a similar

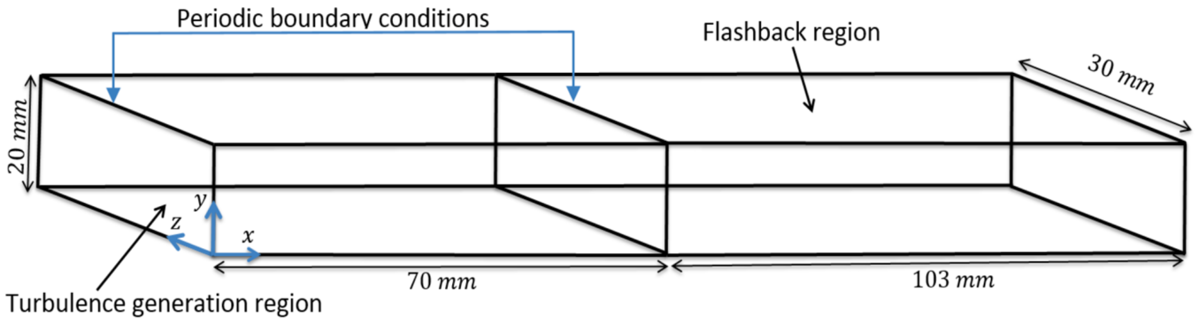

Figure 2. Computational domain in the channel flow region[3,27]

technique as described above. For the results presented below in section 4, only the flashback region of the domain where the flame exists is considered for this analysis. This is due to the gradients of the chemical species (H_2O in the present work) remaining zero outside of this region during the simulation, having no effect on the statistics presented in this study.

3. Mathematical Background and Numerical Implementation

If the reaction zones are assumed to be of the surface-type, the flame-flame interactions can be considered to occur when two flame sheets collide[17]. These flame-flame interactions in turbulent combustion generate local topologies which can be identified by analysing the critical points within the flame in relation to the progress variable[17,20,21]. In this study, a flame sheet is defined based upon the isosurface of the reaction progress variable c, defined as a normalised species mass fraction of water vapor Y_{H2O}:

$$c = \frac{Y_{H_2O} - Y_{H_2O_R}}{Y_{H_2O_P} - Y_{H_2O_R}} \quad (1)$$

with subscripts R and P representing reactant and product sides of the flame, respectively.

It should be made clear that the gradient of the reaction progress variable c is used to evaluate quantities such as the flame normal vector $\underline{n}$, the flame surface curvature κ and the SDF. The gradient of c also vanishes at critical points within the flame. Given this, the Taylor series expansion around a critical point within the flame simplifies to[17,20,21]:

$$c(\boldsymbol{a} + \boldsymbol{x}) = c(\boldsymbol{a}) + (\frac{\boldsymbol{x}^T}{2}) \underline{\underline{H}}(c(\boldsymbol{a}))\boldsymbol{x} + \cdots \quad (2)$$

The FSI topologies can be identified using the signs of the eigenvalues of the Hessian matrix of the reaction progress variable $\underline{\underline{H}}(c)$. The eigenvalues of the Hessian are real, giving the curvature along each of the three orthogonal principal axes[17]. Assuming the orientation is to be considered irrelevant, these eigenvalues fully define the local topology to second order[17].

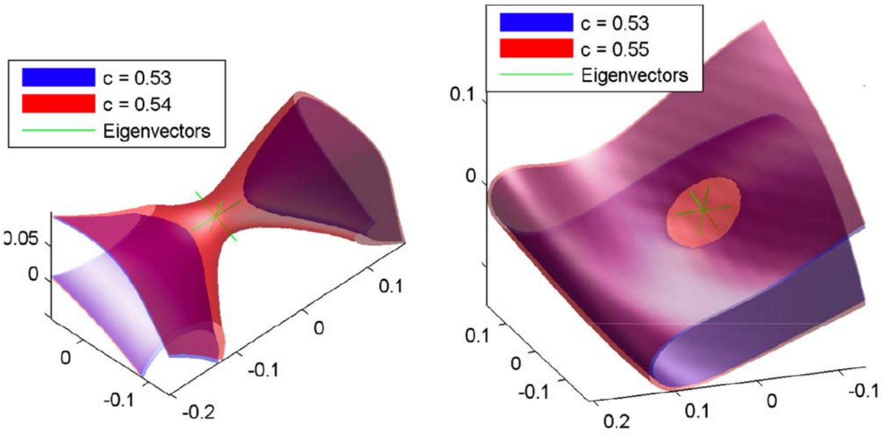

(a) Tunnel Closure (b) Tunnel Formation

Figure 3. Examples of two topologies resulting from flame-self interactions. A tunnel closure topology on the left $(+ - -)$ and a tunnel formation topology on the right $(+ - -)$ obtained from DNS data[17] with all units in mm.

Figure 3a represents a typical tunnel closure FSI topology defined by two positive and one negative eigenvalue which can be seen to feature a significantly different geometry to figure 3b which is a tunnel formation FSI topology consisting of one positive and two negative eigenvalues[17]. Converting the eigenvalues to spherical coordinates gives a more effect method for describing each FSI topology. This is achieved using equations 3-4, where $\lambda_1 > \lambda_2 > \lambda_3$, giving latitude Ø about pole vector $[e_{\lambda_1}, e_{\lambda_2}, e_{\lambda_3}]$ and longitude θ about meridian vector $[e_{\lambda_1}, 0, -e_{\lambda_3}]$ with κ being the magnitude of the eigenvalues (an overall measure of curvature, equation 5)[17]. Equation (3-4) become shape factors[17,20,21] and equation (5) becomes a scaling parameter[17] with dimensions of length^{-2}.

$$\theta = \frac{6}{\pi} tan^{-1}\left(\frac{(\lambda_1 - 2\lambda_2 + \lambda_3)/\sqrt{6}}{(\lambda_1 - \lambda_3)/\sqrt{2}}\right) \quad (3)$$

$$\emptyset = \frac{2}{\pi} tan^{-1}\left(\frac{(\lambda_1 + \lambda_2 + \lambda_3)\cos\left(\frac{\theta\pi}{6}\right)/\sqrt{3}}{(\lambda_1 - \lambda_3)/\sqrt{2}}\right) \quad (4)$$

$$\kappa = \sqrt{(\lambda_1^2 + \lambda_2^2 + \lambda_3^2)} \quad (5)$$

Normalising the shape factors to $\pm$ unity, they can be used to define a continuous two-dimensional domain fully describing the range of local topologies associated with flame self-interactions[17]. For further detail on the aforementioned conversion method used to visually represent the local FSI topologies the reader is directed to reference 17. Figure 4 represents the FSI topology corresponding to a range of example pairs of shape factors in an equirectangular projection of θ and Ø at intervals across their normalised range[17].

Moving across the flame self-interaction topologies described in the $\theta - \emptyset$ space as shown in figure 4, the signs of the eigenvalues of the Hessian of the reaction progress variable $\underline{\underline{H}}(c)$ change from $(- - -)$ to $(- - +)$ to $(- + +)$ to $(+ + +)$ from left to right. The black lines between each colour represent the locus points at which an eigenvalue changes sign. On the left-hand side of figure 4, the eigenvalues with the signs of $(- - -)$ correspond to Burnt Gas Mixture Pockets (BGP) FSI topologies and are outward-propagating spherical flame pockets ('Product Pockets'). Conversely, the topologies with the eigenvalue signs of $(+++)$ on the right-hand side of figure 4 correspond to Unburnt Gas Mixture Pockets (UBGP) and are inward-propagating spherical flame pockets ('Reactant Pockets"). Furthermore, the section of figure 4 two stages in from the left (owning the eigenvalue signs of $(--+)$) correspond to Tunnel Formation (TF) topologies, and the collection of topologies in the section to the right of this again (owning the eigenvalue signs of $(-++)$) correspond to Tunnel Closure (TC) topologies. In a physical sense, the Tunnel Closure (TC) topologies are cylindrical FSI topologies that propagates inwards towards a common axis, whereas the Tunnel Formation (TF) topologies are cylindrical FSI topologies that propagate away from a common axis.

Among the most important events in terms of its effect on the total flame surface area and consequently the overall turbulent burning rate is **flame pinch-off**. Flame Pinch-off occurs by the means of a tunnel closure FSI event and the formation of a reactant pocket (UBGP). Conversely, the tunnel formation event results in the creation of a burnt gas pocket (BGP)[21].

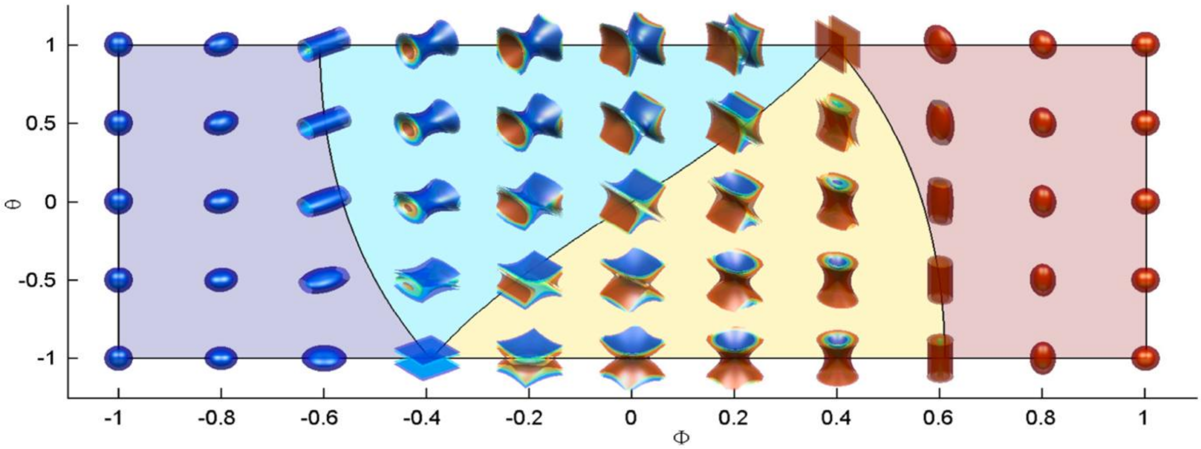

Figure 4. Various types of FSI topologies characterised by the shape factors $\theta$and $\emptyset$. The background colours of the quadrants represent the different types of FSI topology (Dark Blue = BGP $(---)$, Light Blue = TF $(--+)$, Yellow = TC $(-++)$ and Red = UBGP $(+++)$. For colour scheme applied to each topology element, blue represents a relatively colder temperature (low *c*) and red a relatively hotter temperature (high *c*)[17].

The dynamics of the topologies can be further understood by addressing the colour mapping scheme used in figure 4. Blue represents a lower temperature (or lower progress variable) and red represents a higher temperature (higher progress variable). Using this scheme, it is possible to derive the direction of propagation of each element within the flame. Utilising the shape factor domain along with the other relevant variables including the progress variable *c*, the scaling parameter giving a measure of the overall curvature κ and the reaction rate provides the fundamentals required to gather statistical data about the FSI associated with hydrogen-air combustion within the DNS database[17].
It should be noted that in the current analysis, critical points calculated within the flashback region of the domain with progress variable either close to zero or unity, or with a very low curvature, have been filtered out to increase the integrity of the results obtained. FSI statistics are extracted at different wall normal distances (*y/h* = 0.05, 0.1, 0.3, 0.6, 0.95, 1.0) from the DNS of boundary layer flashback of hydrogen-rich combustion. The FSI statistics are conditioned on the reaction progress variable defined in terms of water vapor mass fraction across a range of $0.01 \leq c \leq 0.99$ to ensure only the FSI topologies are investigated in the regions of combustion.

FSI Topology	Eigenvalue Signs	Shape	Direction of Propagation	Background Colour (fig.4)
Burnt Gas Mixture Packet (BGP)	$(---)$	Spherical	Outwards	Dark Blue
Unburnt Gas Mixture Packet (UBGP)	$(+++)$		Inwards	Red
Tunnel Closure (TC)	$(-++)$	Cylindrical	Towards a common axis	Yellow
Tunnel Formation (TF)	$(--+)$		Away from common axis	Light Blue

Table 1. Investigated FSI topologies and their corresponding properties.

4. Results and Discussion

4.1. Flow and Flame Behaviour

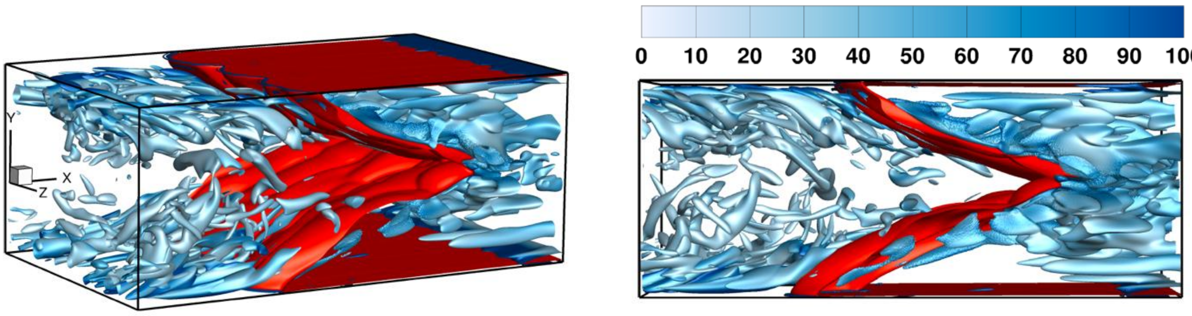

Figure 5. Instantaneous distributions of iso-surfaces of the temperature 1700K (red colour) and the instantaneous normalized vorticity magnitude (blue colour) in the flashback region of the channel. Left figure gives an isometric view and the right give a side view[3]. The colour meter at the top right gives the magnitude of the normalised vorticity.

Figure 5 shows the instantaneous iso-surfaces of the flames' temperature at 1700K and the normalised vorticity magnitude in the flashback region of the computational domain. It is evident from figure 5 that the presence of the flame changes the boundary layer structure, and the magnitude of the turbulence decreases across the flame in the near wall regions, whereas vorticity (i.e., turbulence) is generated in the middle of the channel in the product side of the flame. This happens due to the interface in the middle of the channel between the two different flame branches where the turbulence is lower on the non-reacting side of the flame (left side of the flame)[3,41].

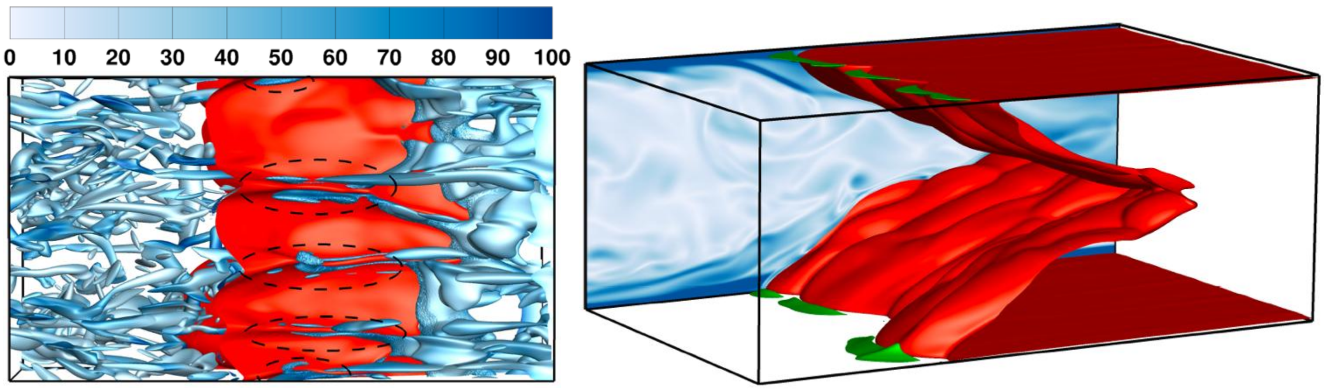

Figure 6. Same conditions apply as *figure 5.* The left figure shows the region near the top wall where the dotted ellipses highlight the regions of flame generated turbulence. The right figure shows the instantaneous normalised viscosity along with the regions of negative flow shown with green iso-surfaces[3].

Figure 6 (left) shows a snapshot of the channel flow from the top view. Note the iso-surfaces of the temperature close to the top wall boundary are removed to show the vorticity magnitude. It is evident from figure 6 (left) that local cusps are formed on the flames surface towards the product side. These cusps are a result of the flame propagating into regions of lower flow velocity at the boundary layer. This velocity gradient is caused by the oncoming flow of reactants and these cusps are seen to generate local turbulence which grows further downstream of the channel[3].

The green iso-surfaces seen in Figure 6 (right) show the highly localised regions where the flow experiences an upstream propagation. These regions of reverse flow are visible immediately upstream of each flame bulge and are localised to only the near-wall boundary layer regions. An earlier study by Gruber *et al*[5] found similar results describing the aforementioned phenomena. The existence of these regions of reverse flow immediately upstream of the flame bulges can be explained by the existence of an adverse pressure gradient. This positive pressure gradient is due to the variation of the pressure field in the near wall region due to the existence of the flame, which ultimately causes flow to propagate upstream towards the reactants[3,5]. Readers are directed to Gruber *et al*[5] for a more in-depth explanation of the mechanisms causing this phenomenon.

The following subsections in section 4 will discuss the properties of the different FSI topologies occurring at different distances from the boundary layer wall by extracting layers of data from the DNS dataset described in section 2. Data was extracted at different y/h values from the boundary layer wall through to the middle of the channel flow and was processed using the methodology described in section 3. A suitable progress variable c based off the mass fraction of water vapor (Y_{H_2O}) was defined to close the unclosed mean/filtered reaction rate as described in section 1.2 and 3. It should be noted that the choice of species used to define the progress variable is relatively unimportant for the following analysis methods providing it is continuous and monotonic[17].

Layer	*y/h* (dimensionless)	Distance from Boundary Layer Wall (mm)
1	0.05	0.5
2	0.10	1.0
3	0.30	3.0
4	0.60	6.0
5	0.95	9.5
6	1.00	10.0

Table 2. Values of y/h (corresponding to distance from the lower wall) investigated for the occurrence of FSI Topologies.

Table 2 displays the different *y/h* layers at which data was extracted from the DNS database and used for analysis in this report. The first two layers were chosen as the aim of this study is to investigate the FSI topology occurrences at the walls' boundary layer during transient flashback, giving information on the topologies 0.5 mm and 1.0 mm from the lower wall. The remaining y/h values proved to give the most interesting results as explained in section 4.5 and describe the overall development of the flame as it progresses away from the wall towards the middle of the channel flow (layer 6). It is important to note insufficient data was available to analyse the FSI topologies at y/h = 0 (i.e., on the wall itself) so this layer is ignored in the current study.

4.2. Probability Density Function Plots.

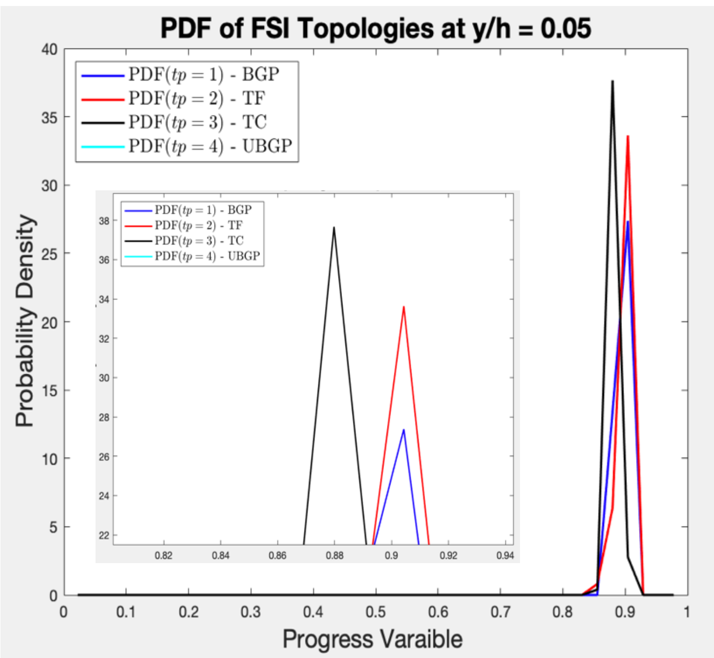

Figure 7 (a)

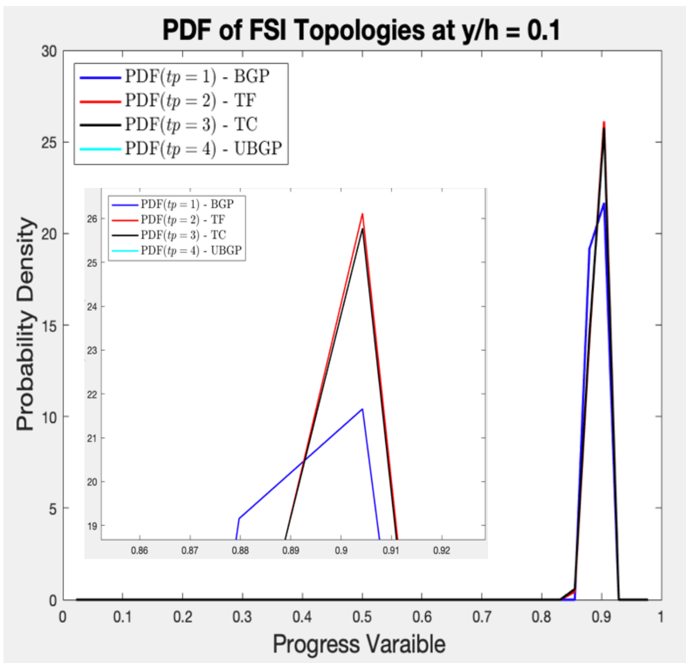

Figure 7 (b)

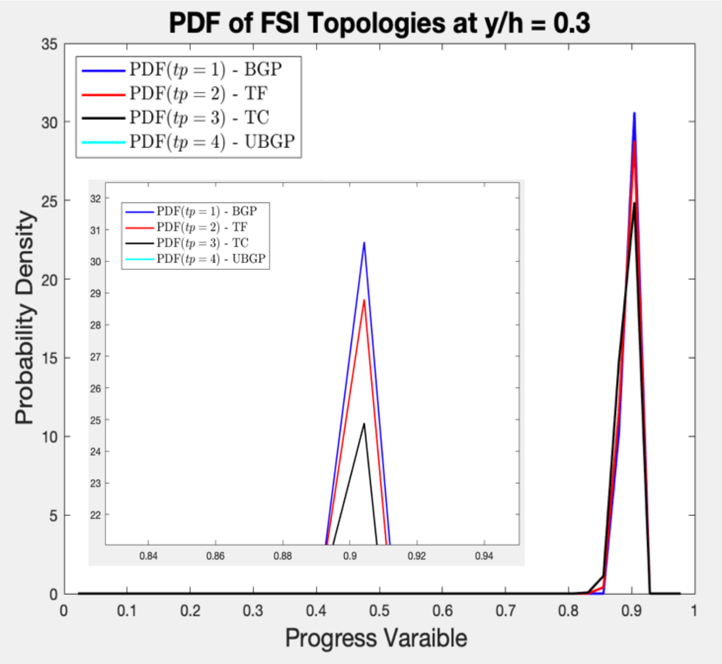

Figure 7 (c)

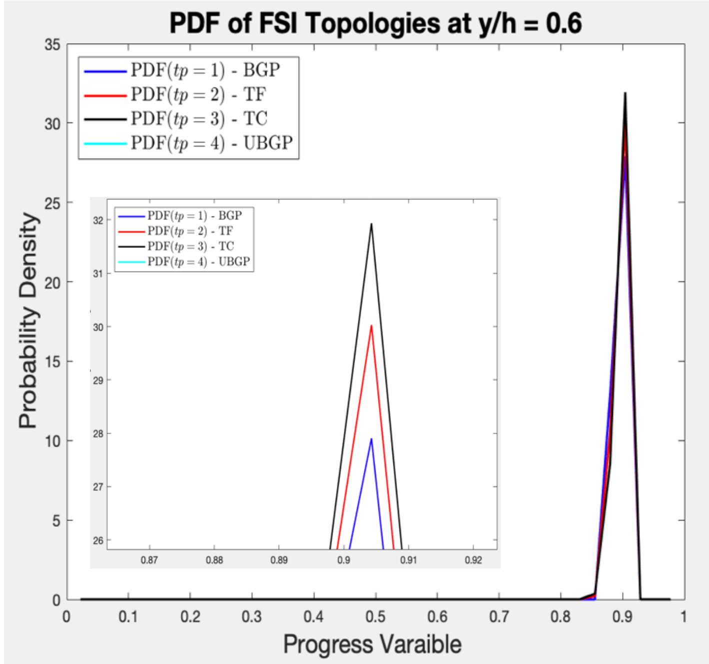

Figure 7 (d)

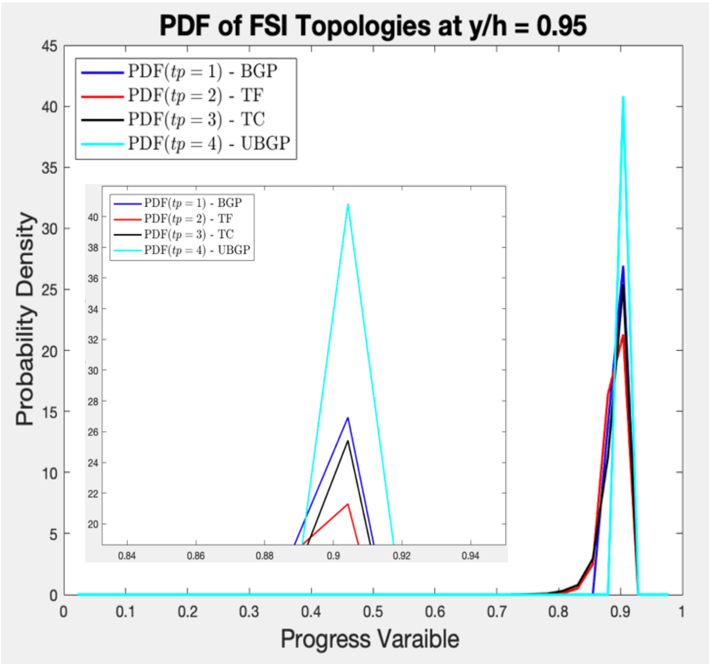

Figure 7 (e)

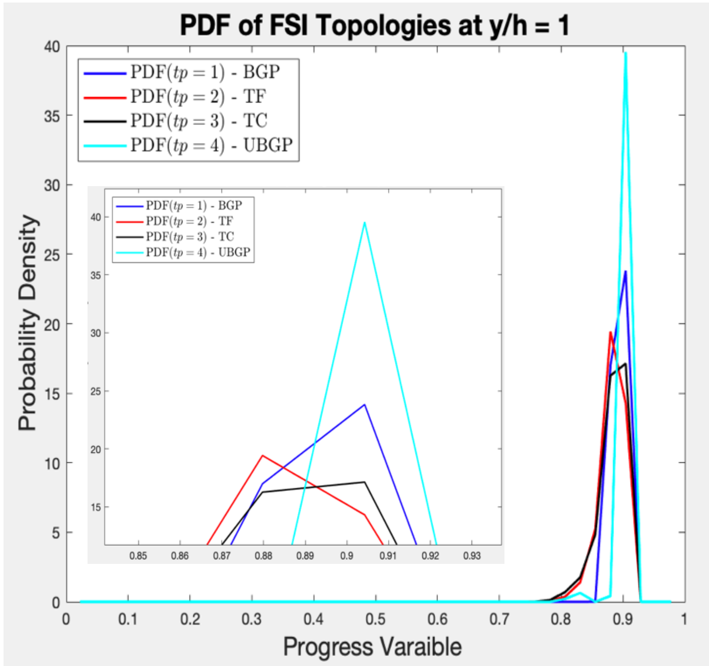

Figure 7 (f)

Figure 7. Probability Density Functions of different FSI Topology types within $0.01 \le c \le 0.99$ at (a) *y/h* = 0.05, (b) y/h = 0.1, (c) y/h = 0.3, (d) y/h = 0.6, (e) y/h = 0.95, (f) y/h =1.

Figure 7 shows PDF plots representing the probability of different FSI topology types occurring within the region where combustion occurs (i.e., $0.01 \le c \le 0.99$) at different wall normal distances from the wall considered within this current study as seen in table 2. It is evident from figure 7 that nearly all FSI topologies are isolated to the trailing edge of the flame ($0.85 \le c \le 0.99$) with the exception of flow near at channels' half height (figure 7f) where a very small number occur slightly before ($c \approx 7.5$). Figure 7 (e-f) shows Unburnt Gas Pockets (UBGP) exist only close to the channel half height (y/h = 0.95-1.0), whereas the remaining topologies (TF, TC, BGP) exist at all locations within the channel flow, again, constrained to the trailing edge of the flame.

4.3. Scatter Plots of FSI Topologies in $\theta - \emptyset$ Domain

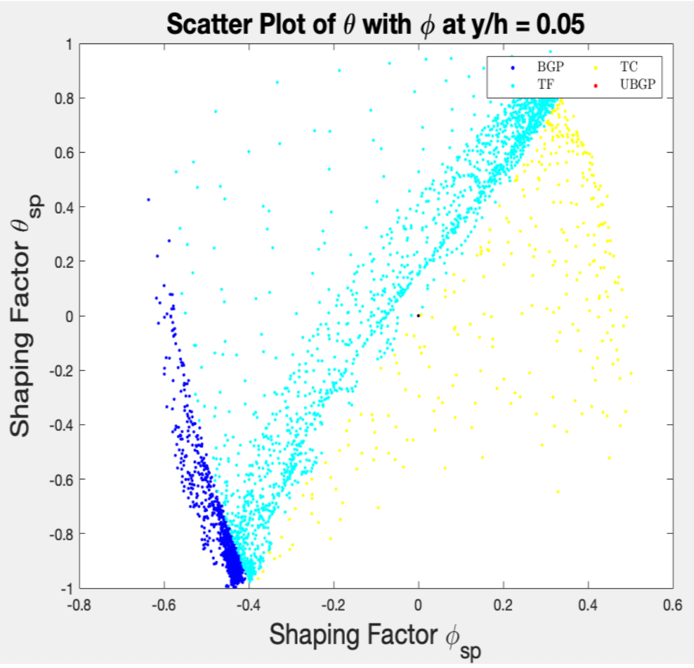

Figure 8 (a)

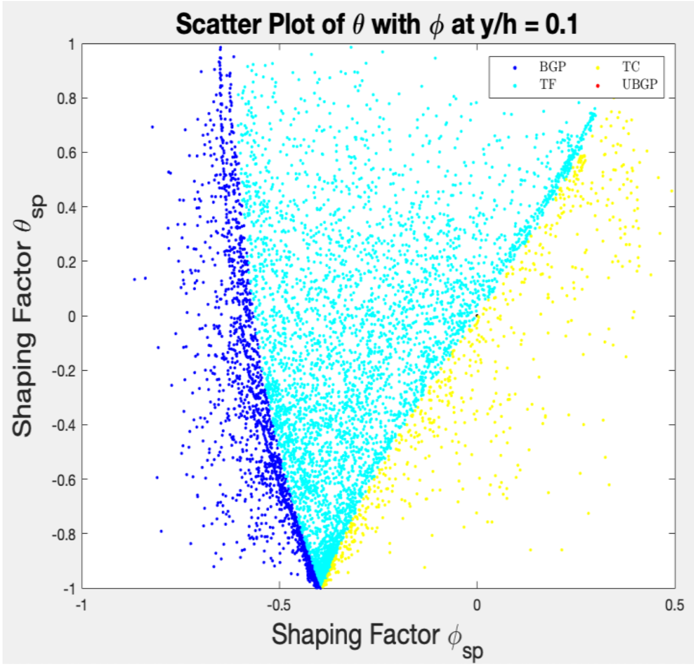

Figure 8 (b)

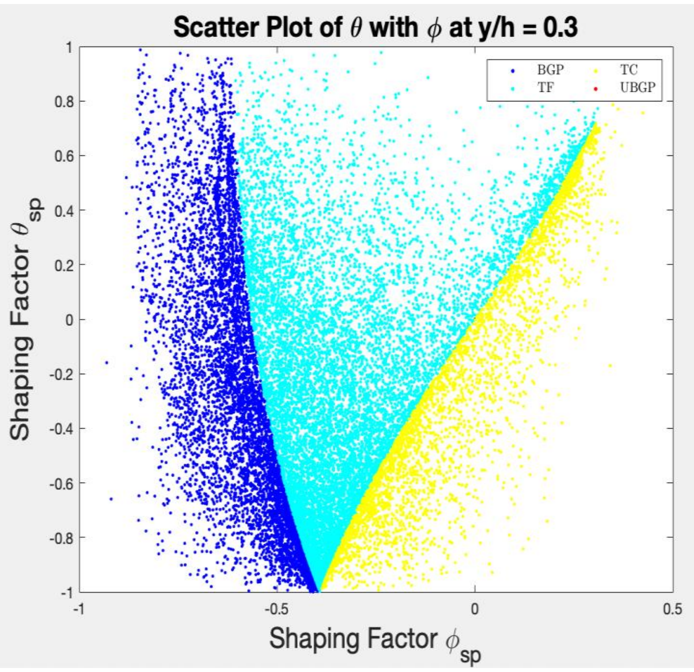

Figure 8 (c)

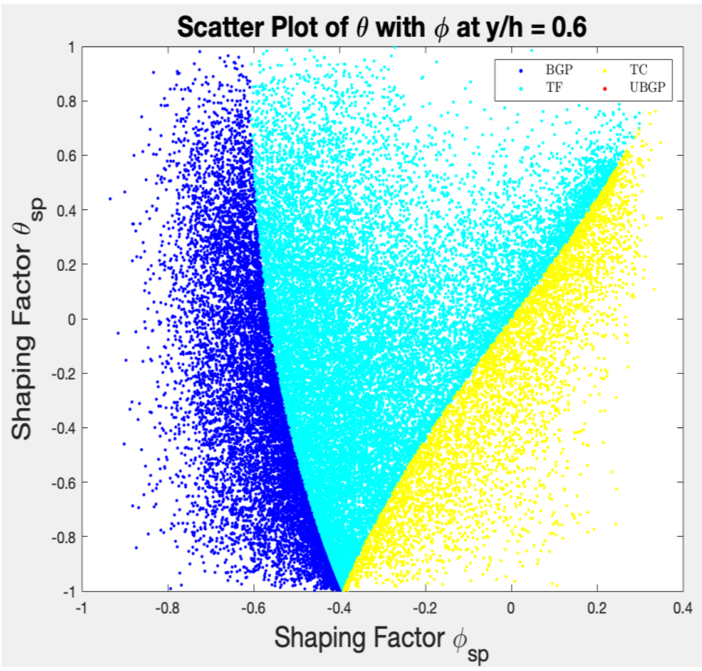

Figure 8 (d)

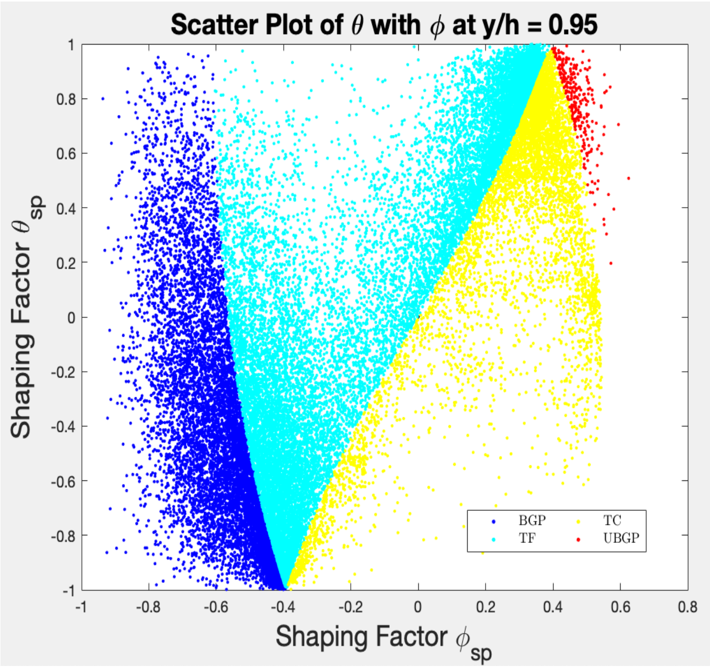

Figure 8 (e)

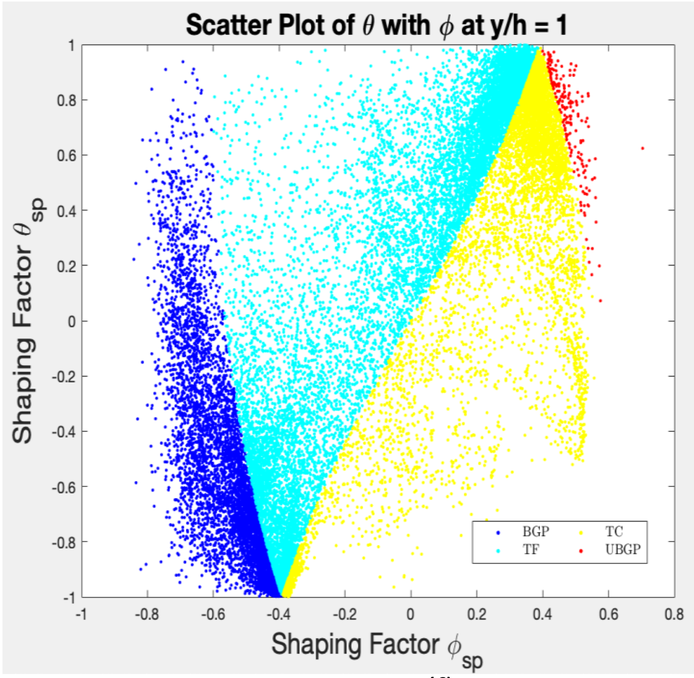

Figure 8 (f)

Figure 8. Scatters Plots of different FSI Topologies in $\theta - \emptyset$ space for $0.01 \leq c \leq 0.99$ at (a) *y/h* = 0.05, (b) y/h = 0.1, (c) y/h = 0.3, (d) y/h = 0.6, (e) y/h = 0.95, (f) y/h =1. (Red = UBGP, Blue = BGP, Cyan = TF, Yellow = TC)

Figure 8 shows scatter plots of the frequency of occurrence of the FSI topologies in the shape factors θ *and* $\emptyset$ domain at different y/h locations considered in this study as outlined in table 2. The scatter plot is colour coded to represent the different topology types for progress variable $0.01 \leq c \leq 0.99$ and uses the same colour coding as figure 4. Lighter areas on the density plot indicate a lower existence of topologies, whereas darker areas represent more FSI topologies occurring within that y/h layer of the flame. From figure 8 it is evident the FSI events are clustered along the locus of points where the eigenvalues of $\underline{\underline{H}}(c)$ change sign. This can be explained due to the increased frequency of topologies which are predominantly two-dimensional, such as two ridges meeting or the expansion/contraction of a cylindrical tunnel of products/reactants[17]. It can be seen from figure 8 (e,f) that Unburnt Gas Pocket's (UBGP) topologies are constrained to occurring only at locations near the middle of the channel flow and this is in agreement with figure 7. The remaining topologies (BGP, TF, TC) are seen at all wall normal distances throughout the channel flow, with their frequency of occurrence increasing towards the middle of the channel.

There are very few FSI topologies 0.5 mm from the boundary layer (y/h = 0.05, figure 8a) relative to interactions 6 mm from the boundary layer (y/h = 0.6, figure 8d). This can be explained due to a larger magnitude of velocity and turbulence at y/h = 0.6 and a lower level of turbulence (and velocity due to the applied no-slip isothermal boundary condition) at the boundary layer y/h = 0.05 as seen on figure 6, indicated by the blue iso-surfaces. Turbulence causes the flame sheet to wrinkle and collide with itself, resulting in a flame self-interaction and generating an FSI event.

4.4. Histogram Plots of FSI Topologies.

4.4.1. Histogram Plots for y/h = 0.05

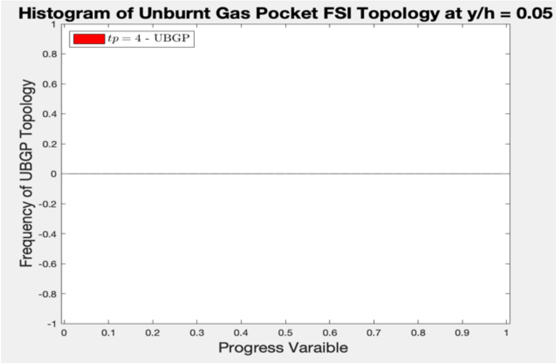

Figure 9 (a.i)

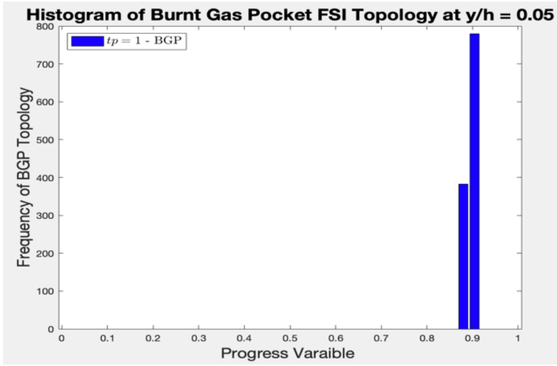

Figure 9 (a.ii)

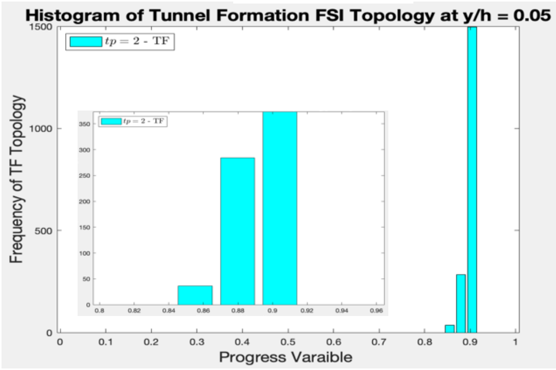

Figure 9 (a.iii)

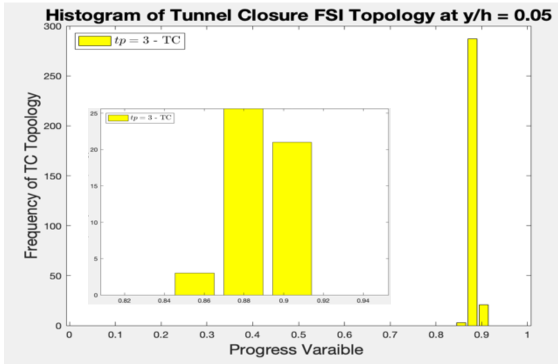

Figure 9 (a.iv)

4.4.2. Histogram Plots for y/h = 0.1

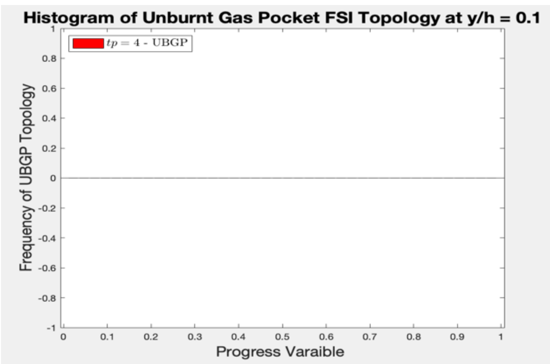

Figure 9 (b.i)

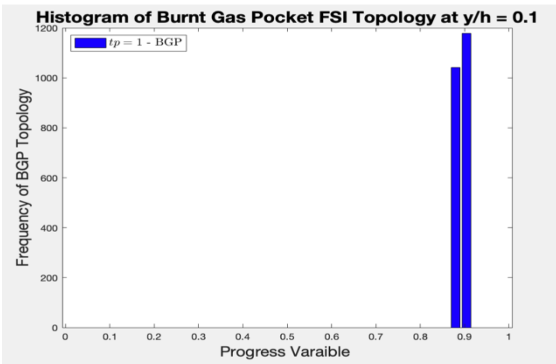

Figure 9 (b.ii)

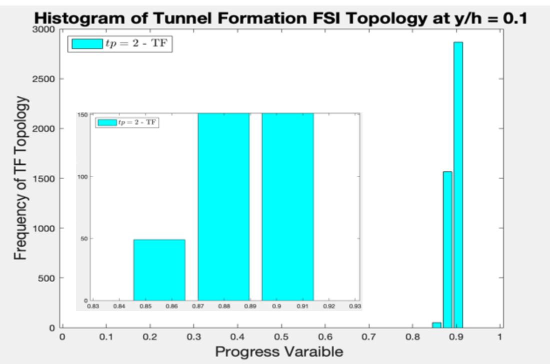

Figure 9 (b.iii)

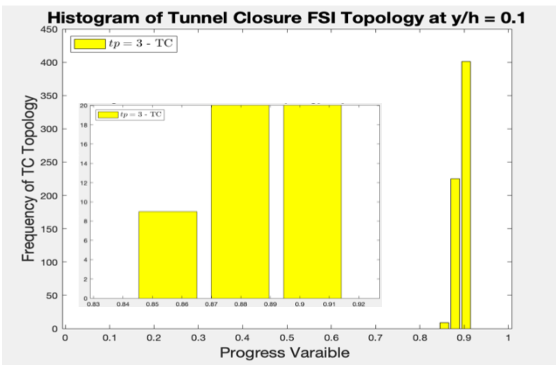

Figure 9 (b.iv)

4.4.3. Histogram Plots for y/h = 0.3

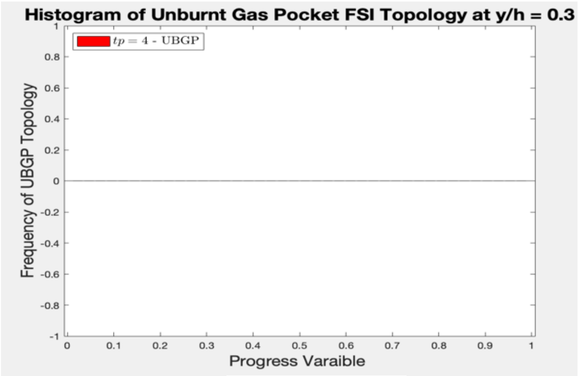

Figure 9 (c.i)

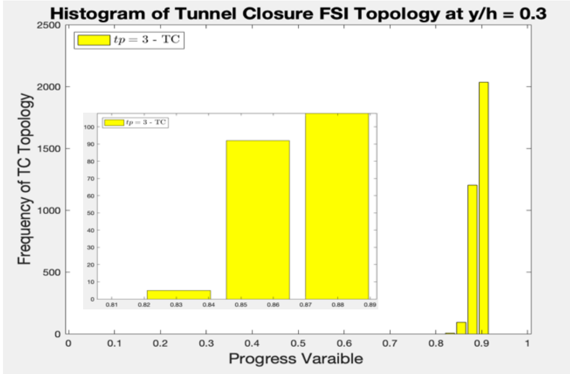

Figure 9 (c.ii)

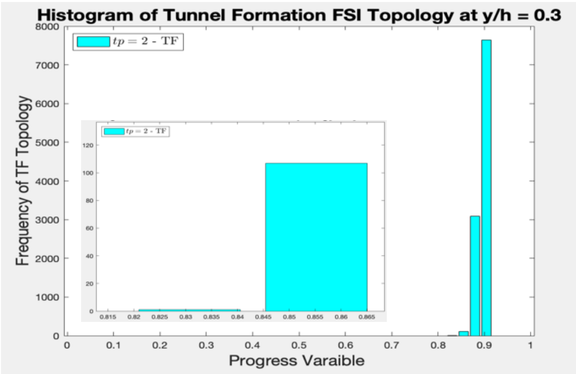

Figure 9 (c.iii)

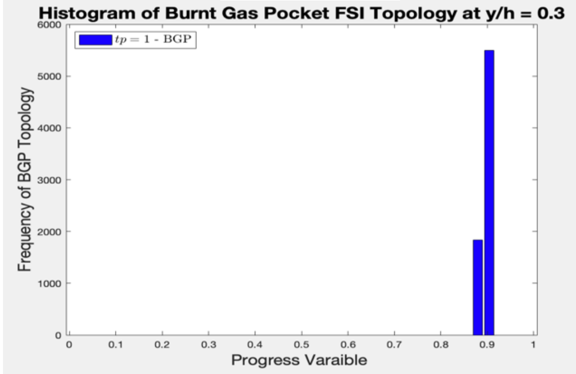

Figure 9 (c.iv)

4.4.4. Histogram Plots for y/h = 0.6

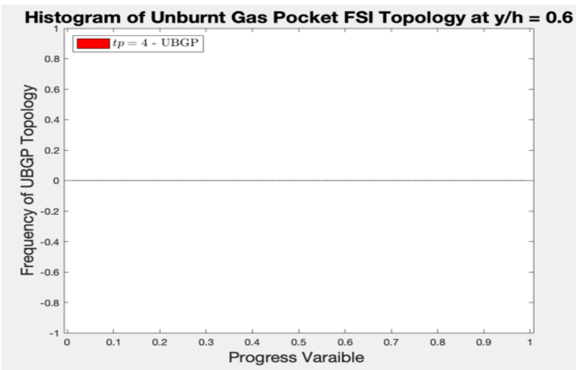

Figure 9 (d.i)

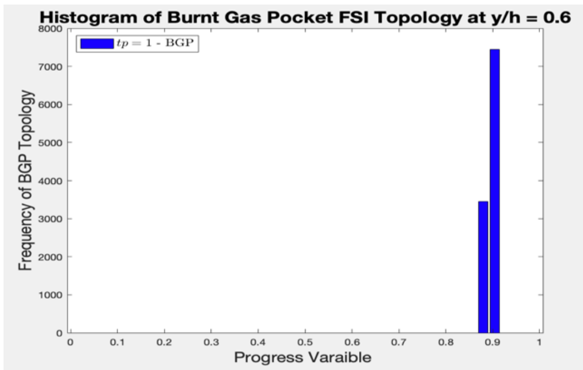

Figure 9 (d.ii)

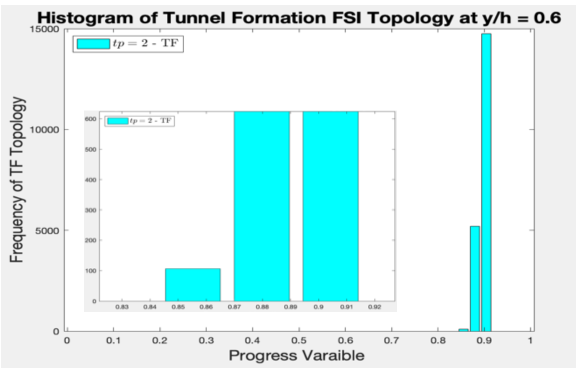

Figure 9 (d.iii)

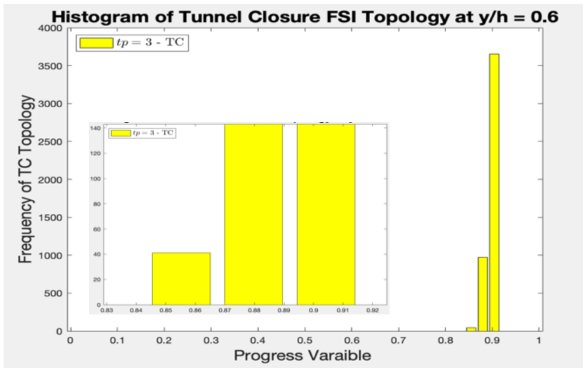

Figure 9 (d.iv)

4.4.5. Histogram Plots for y/h = 0.95

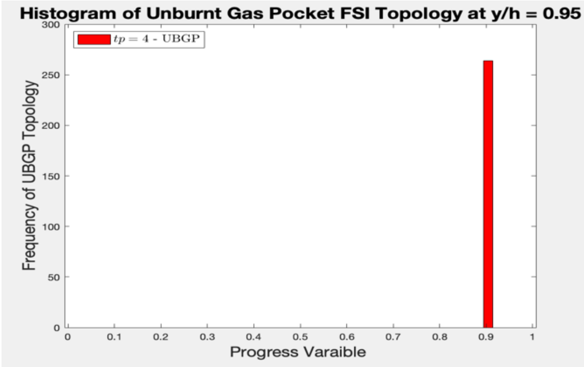

Figure 9 (e.i)

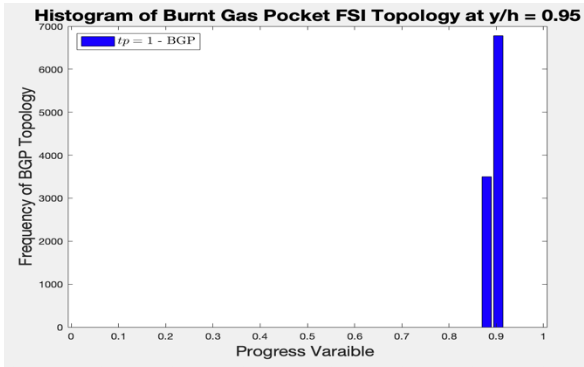

Figure 9 (e.ii)

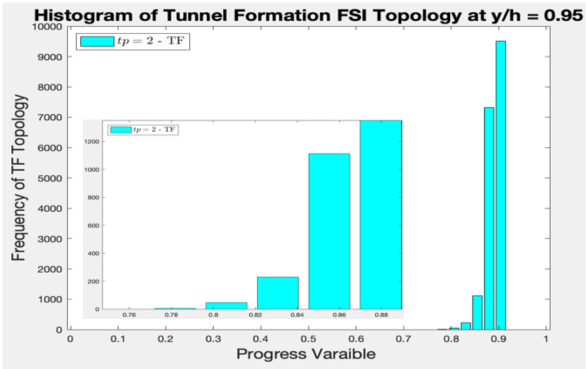

Figure 9 (e.iii)

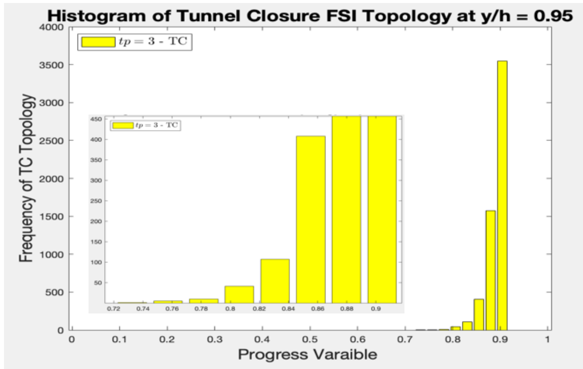

Figure 9 (e.iv)

4.4.6. Histogram Plots for y/h = 1.00

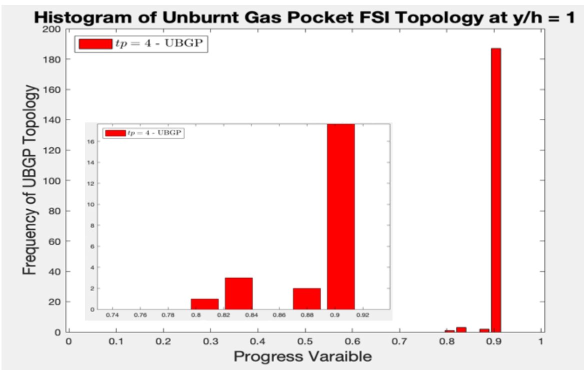

Figure 9 (f.i)

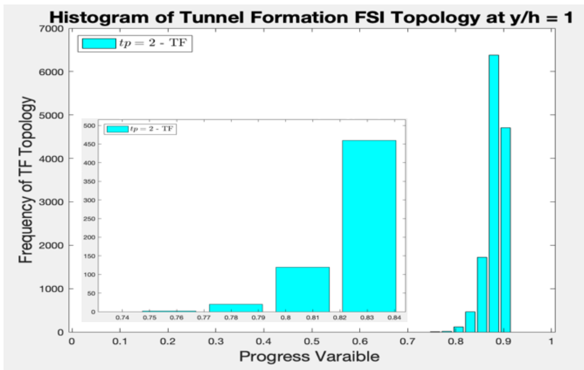

Figure 9 (f.ii)

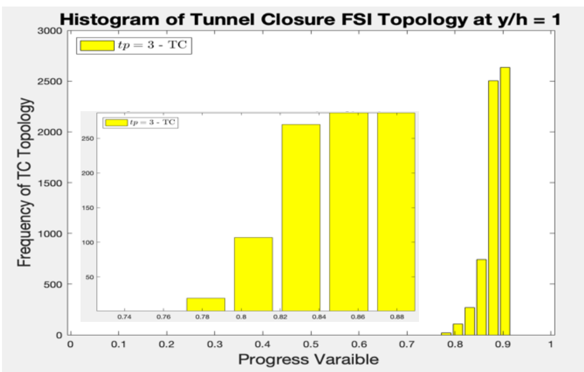

Figure 9 (f.iii)

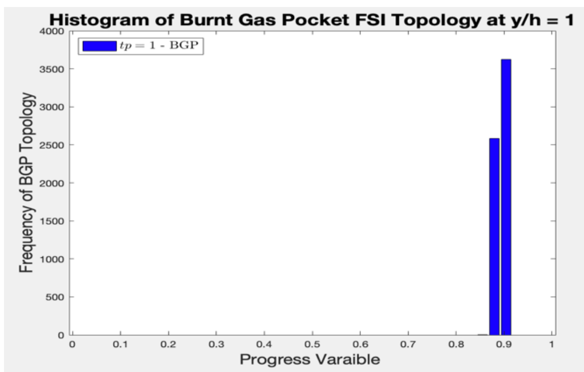

Figure 9 (f.iv)

Figure 9. Histograms with insets at lower frequencies of four different FSI topologies across $0.01 \leq c \leq 0.99$ at (a) *y/h* = 0.05, (b) y/h = 0.1, (c) y/h = 0.3, (d) y/h = 0.6, (e) y/h = 0.95, (f) y/h =1.
The colour of each bar corresponds to: Red (i) = UBGP, Cyan (ii) = TF, Yellow (iii) = TC, Blue (iv) = BGP

4.4.7. Stacked Histogram Plots

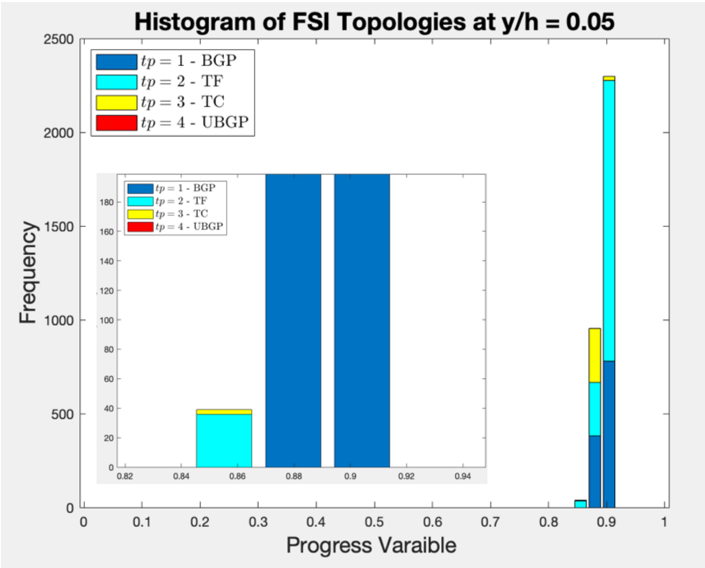

Figure 10 (a)

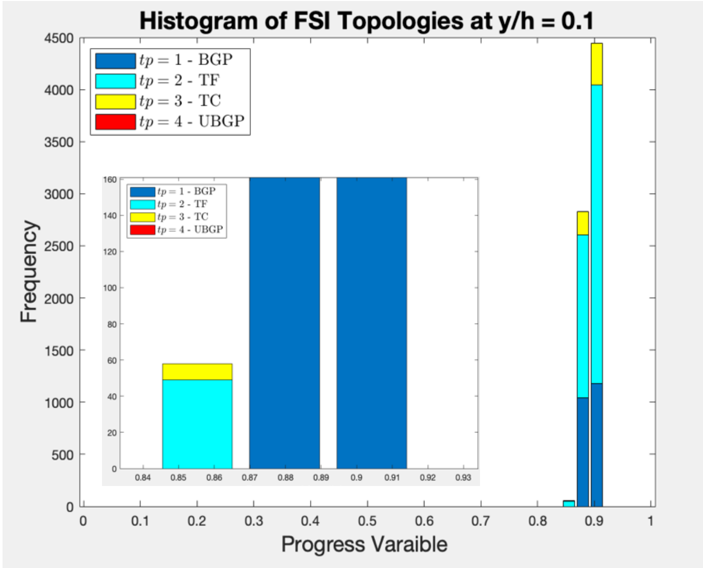

Figure 10 (b)

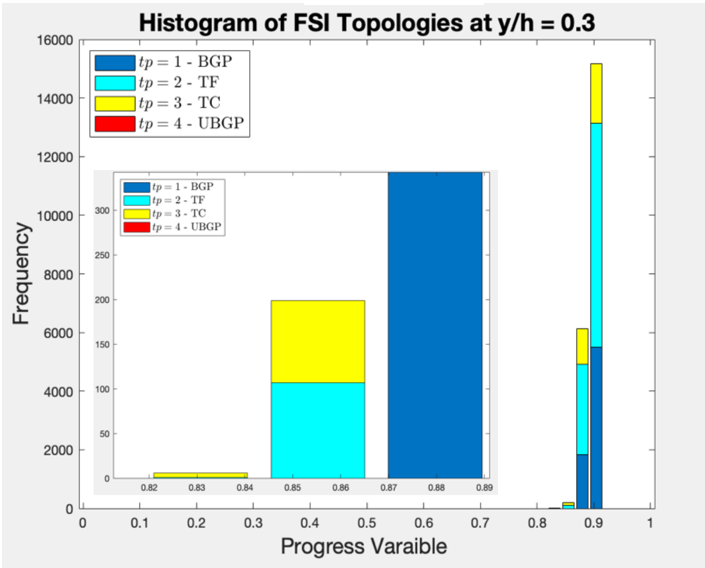

Figure 10 (c)

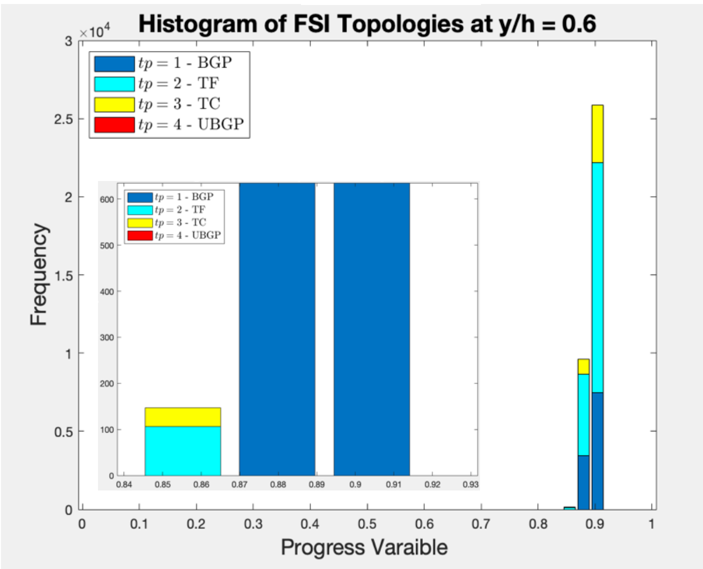

Figure 10 (d)

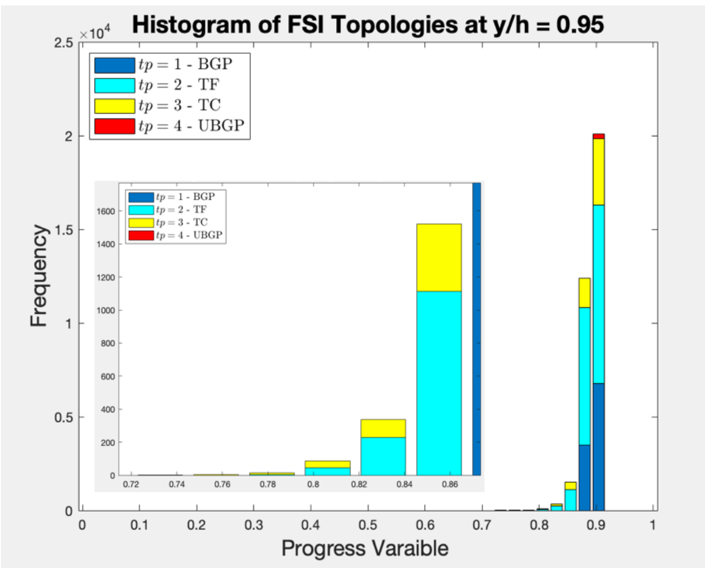

Figure 10 (e)

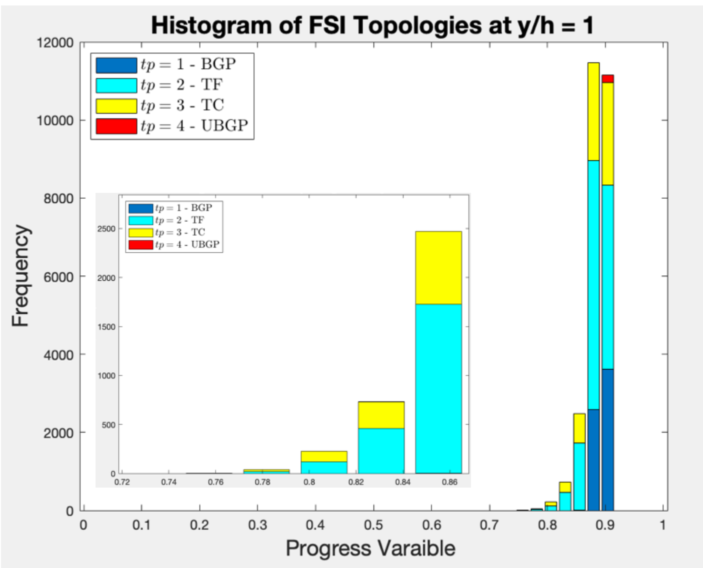

Figure 10 (f)

Figure 9. Stacked histograms with insets at lower frequencies of four different FSI topologies across $0.01 \leq c \leq 0.99$ at (a) *y/h* = 0.05, (b) y/h = 0.1, (c) y/h = 0.3, (d) y/h = 0.6, (e) y/h = 0.95, (f) y/h =1.
The colour of each bar corresponds to: Red = UBGP, Cyan = TF, Yellow = TC, Blue = BGP

4.4.8 Histograms of FSI Topologies Discussion

Figure 8 and 9 shows the histograms of the FSI topologies across $0.01 \leq c \leq 0.99$ for all wall normal distances considered within this study (i.e., y/h = 0.05, 0.1, 0.3, 0.6, 0.95, 1.0). The FSI topologies have been based of the critical points of the Hessian matrix of the reaction progress variable *c* and the sign of their eigenvalues. The type of each of the critical points (FSI topologies) is represented on the histograms as a different colour, that being: Red = UBGP, Cyan = TF, Yellow = TC, Blue = BGP. The flame-flame interaction types are shown in figure 4 along with examples of the Tunnel Formation (TF) and Tunnel Closure (TC) topologies given in figure 3. Each of these topologies were explained qualitatively in Section 3.

All the plots in figures 9 and 10 are monomodal indicating the FSI topologies exist in a very confined region within the flame at all axial positions within the channel flow. It is evident from figure 10 that all FSI events occur only towards the burned gas region $0.75 \leq c \leq 0.99$ or the trailing edge of the turbulent flame brush at all distances from the boundary layer wall. The strong majority of FSI events occur in the region of $0.85 \leq c \leq 0.99$ which is to be expected due to the relatively large reaction rate preceding this which corresponds to a larger rate of change of progress variable $|\nabla c|$ and consequently a lower probability of encountering a flame self-interaction from a single snapshot of the domain at a single instance in time. Local alignment of the progress variables' iso-surface normal with the most compressive principal strain rate increases as progression is made from the leading to the trailing edge (low to high progress variable) of the turbulent flame brush[53]. The over-all net effect of the aforementioned conditions is to increase the propensity of interactions towards the trailing edge of the turbulent flame brush[17]. It should be noted that the aforementioned observations are similar qualitatively to the findings for globally stoichiometric spherically expanding flames propagating into fuel droplet-mists for different turbulence intensities[52].

Figures 9 and 10 show no FSI events in the region of the flame proceeding C = 0.75 at any instance within the channel flow which is in disagreement of the behaviours seen in a previous study by Griffiths et al[17] of a turbulent premixed freely propagating hydrogen jet flame, where there were significant FSI events found towards the unburned gas regions (low progress variable) of the flame. These differences in the location of FSI events within the flame region is not unexpected giving the physical differences the boundary layer wall introduces, and these discrepancies must be taken into consideration particularly when formulating models for premixed turbulent boundary layer flashback.

It is clear from figure 10 that the UBGP events are extremely rare in comparison to the remaining topologies (BGP, TF, TC) and can only be found towards the middle of the turbulent channel flow at *y/h* = 0.95 to *y/h* = 1. They are isolated to the trailing edge of the flame brush ($c = 0.9$) and account for a very small quantity of overall FSI occurrences. The lack of UBGP occurrences can be explained due to the transient nature of such an event. With these topologies being surrounded on all sides by hot burnt gas pockets (BGP), the unburned gas pockets (UBGP) are rapidly consumed[10,20,55], making the probability of observing such an event extremely low with one snapshot at a single instance in time. Flame pinch-off is a result of a tunnel closure event and produces an isolated UBGP. From figure 10 it is clear that UBGPs occur only towards the middle of the channel flow where the flow velocity is at a maximum. The larger the magnitude of the flow velocity, the more likely of a flame pinch-off event occurring to producing an UBGP. This further explains why such an event is isolated to the higher velocity regions in the middle of the channel flow. This rarity of UBGPs is consistent with the finding from a previous analysis of FSI interactions in turbulent premixed gaseous flames conditioned under different turbulence intensities by Trivedi *et al*[20].

4.5. Percentage and Overall Occurrences of FSI Topologies

Table 3 shows the quantity of each type of FSI event within the region of combustion (i.e., $0.01 \leq c \leq 0.99$) at different *y/h* values and consequently at different distances from the boundary layer wall, through to the middle of the channel flow. It is clear from table 3 that FSI events are least frequent at the vicinity of the wall (*y/h* = 0 to *y/h* = 0.1) and the propensity of an FSI event occurring increases as progression is made towards the centre of the channel flow, until *y/h* = 0.7. A decrease in the frequency of these events is then observed above 7 mm from the lower wall (*y/h* = 0.7) up until the middle of the channel flow at *y/h* = 1. This observation is a consequence of the variation of the flow velocity throughout the channel.

		FSI Topologies Frequency of Occurrence				
Distance from Wall (mm)	y/h	BGP	TF	TC	UBGP	SUM
0.0	0.00	0	0	0	0	0
0.5	0.05	1163	1817	331	0	3291
1.0	0.10	2220	4479	635	0	7334
2.0	0.20	4217	9841	2733	0	16791
3.0	0.30	7332	10842	3334	0	21508
4.0	0.40	7417	14253	3081	0	24751
5.0	0.50	9736	16797	2784	0	29317
6.0	0.60	10892	20044	4570	0	35606
7.0	0.70	10995	21944	4670	0	39501
8.0	0.80	13922	20647	3067	0	37636
9.0	0.90	13021	16853	3778	20	33672
9.5	0.95	10276	18236	5691	264	34467
10.0	1.00	6279	13418	6205	193	26095

Table 3. The frequency of occurrences of each type of FSI events within $0.01 \leq c \leq 0.99$ at different distances from the boundary layer wall.

Table 4 shows the percentage weighing of each type of FSI topology at different distances from the boundary layer wall. It is evident that the most predominant event is Tunnel Formation, consistently accounting for over 50% of all topologies at all wall normal distances. This is followed by Burnt Gas Pockets being the 2nd most frequent, then Tunnel Closures third, and finally Unburnt Gas Pockets consistently being the rarest with no occurrences until *y/h* = 0.9. It is interesting to note that this frequency hierarchy is consistent throughout the channel flow at all *y/h* values and is never broken.

		Percentage Weighing of FSI Topologies			
Distance from Wall (mm)	y/h	BGP (%)	TF (%)	TC (%)	UBGP (%)
0.00	0.00	0	0	0	0
0.5	0.05	35	55	10	0
1.0	0.10	30	62	8	0
2.0	0.20	25	58	17	0
3.0	0.30	34	51	15	0
4.0	0.40	30	57	13	0
5.0	0.50	33	57	10	0
6.0	0.60	30	56	14	0
7.0	0.70	28	56	16	0
8.0	0.80	37	55	8	0
9.0	0.90	38.67	50.05	11.22	0.06
9.5	0.95	29.81	52.91	16.51	0.77
10.0	1.00	24.06	51.42	23.78	0.74

Table 4. The percentage weighing of each type of FSI event within $0.01 \leq c \leq 0.99$ at different distances from the boundary layer wall.

Graph 1 shows the frequency of each FSI topology at different distances from the wall along with the overall frequency of interactions. It is evident from Graph 1 that the TF topology is consistently the prevalent FSI event at all wall normal distances throughout the channel, followed by the BGP type then the TC type, and finally the UBGP proves to be the rarest event only existing towards the middle of the channel. Furthermore, Graph 1 shows that the overall frequency of interactions increases to a maximum at y/h = 0.7, then slowly decreases towards the region at the middle of the channel flow. Graph 2 shows the percentage weight attached to each topology type at different distances from the wall boundary. It is clear from Graph 2 that the frequency hierarchy $TF_f > BGP_f > TC_f > UBGP_f$ (with subscript f meaning frequency) is consistent at all distances from the wall. It should be noted the aforementioned hierarchy is inconsistent with two previous studies of an open turbulent premixed jet spray flame[16] and a freely propagating premixed flame in shear generated turbulence[49]. Both of these mentioned studies mutually agree on a topology frequency hierarchy $TF_f > TC_f > BGP_f > UBGP_f$. Another study on spherically expanding premixed gaseous flames at different turbulence intensities[52] describes a frequency hierarchy of $BGP_f > TF_f > TC_f > UBGP_f$. These variations of the most predominant topology type is not unexpected giving the physical differences the turbulent boundary layer introduces to the flow in comparison to freely propagating flames or droplet laden mixtures, and these discrepancies must be taken into consideration particularly when formulating models for premixed turbulent boundary layer flashback.

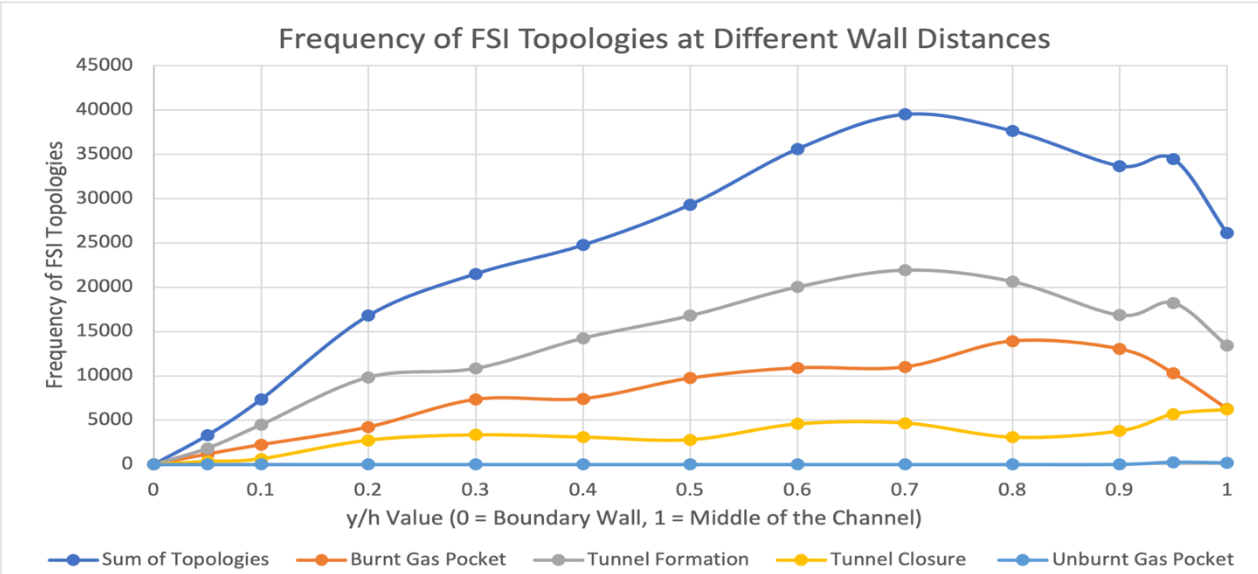

Graph 1. The frequency of occurrences of each type of FSI events and accumulative frequency within $0.01 \leq c \leq 0.99$ at different distances from the boundary layer wall.

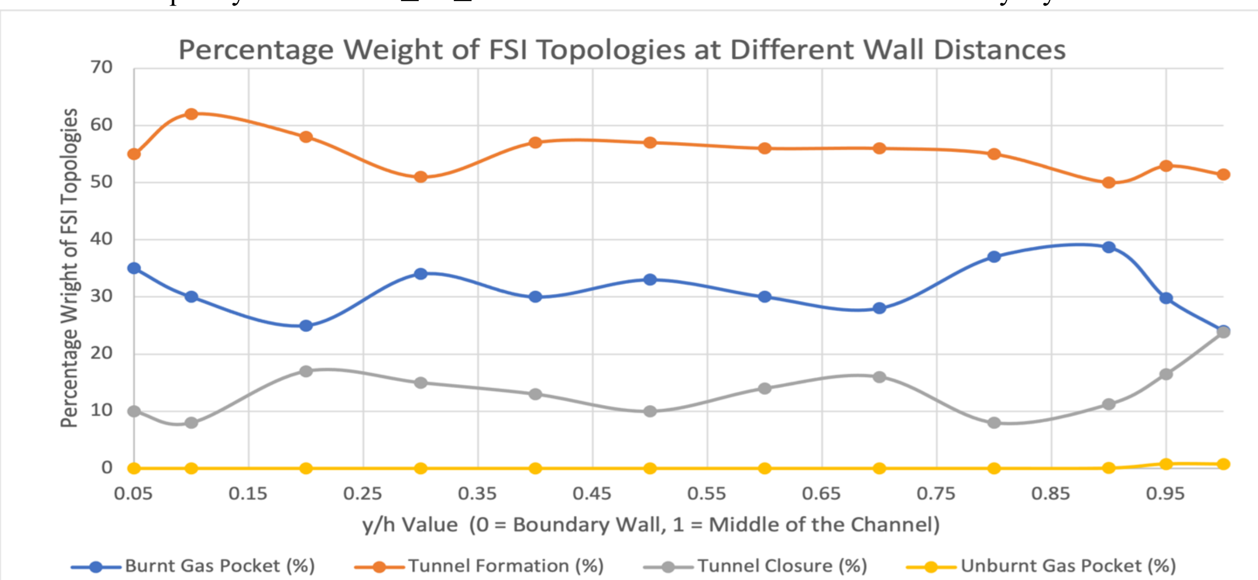

Graph 2. The percentage weighing of each type of FSI event within $0.01 \leq c \leq 0.99$ at different distances from the boundary layer wall.

4.6. Mean and Gaussian Curvatures

4.6.1. Mean and Gaussian Curvatures at y/h = 0.05

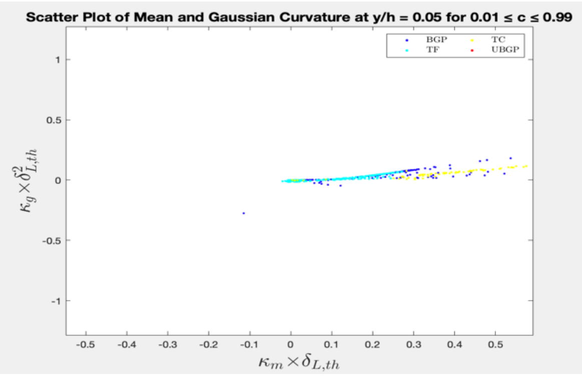

Figure 11 (a.i)

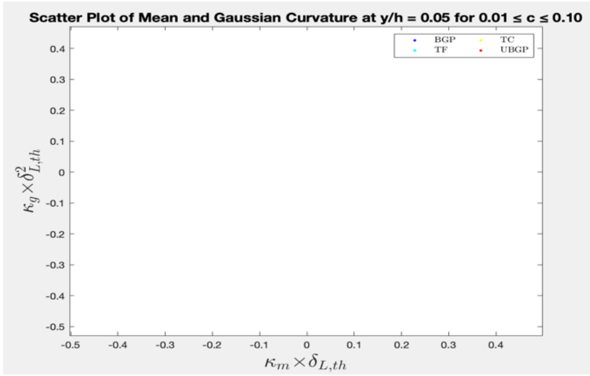

Figure 11 (a.ii)

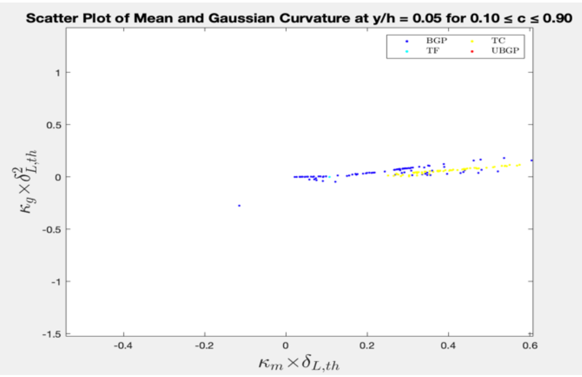

Figure 11 (a.iii)

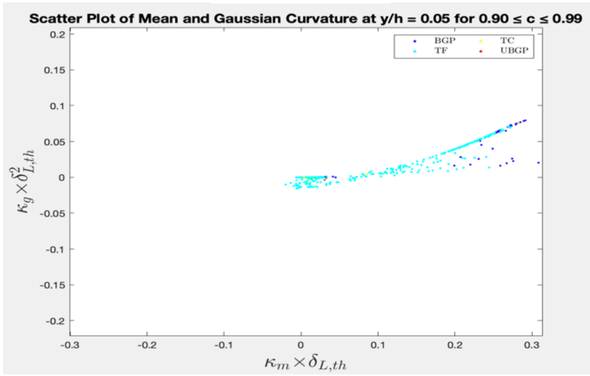

Figure 11 (a.iv)

4.6.2. Mean and Gaussian Curvatures at y/h = 0.1

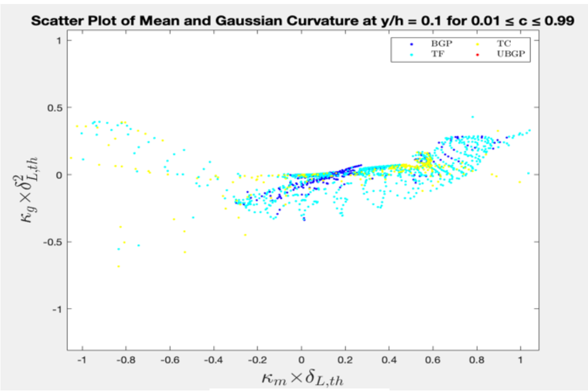

Figure 11 (b.i)

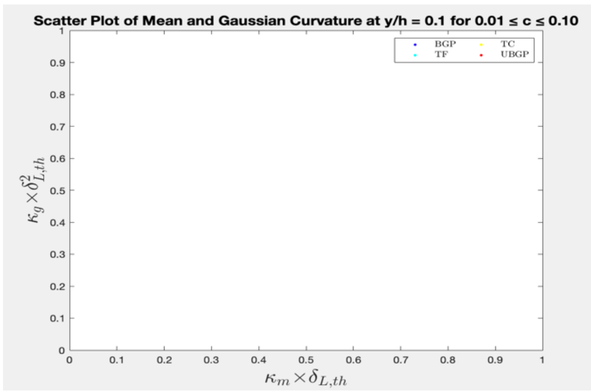

Figure 11 (b.ii)

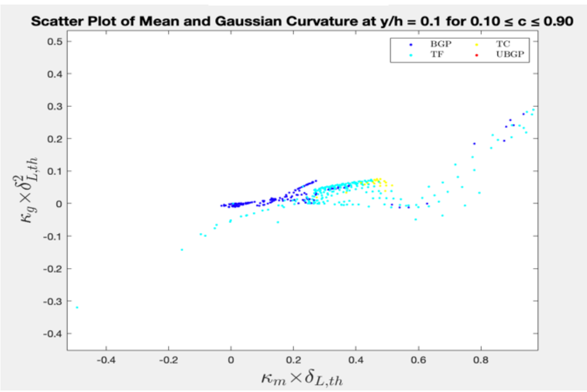

Figure 11 (b.iii)

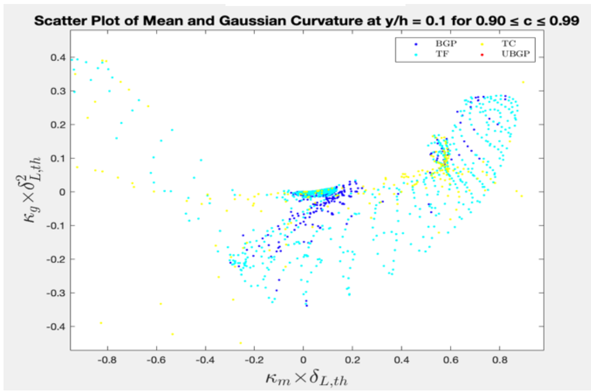

Figure 11 (b.iv)

4.6.3. Mean and Gaussian Curvatures at y/h = 0.3

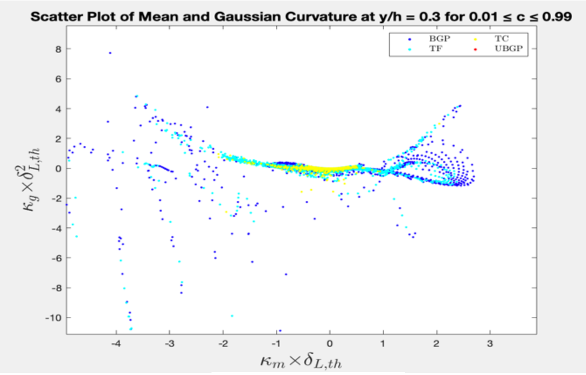

Figure 11 (c.i)

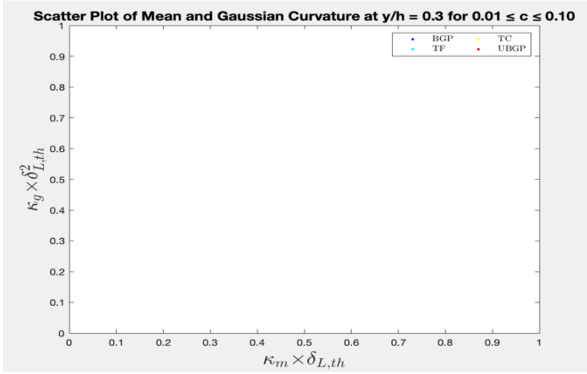

Figure 11 (c.ii)

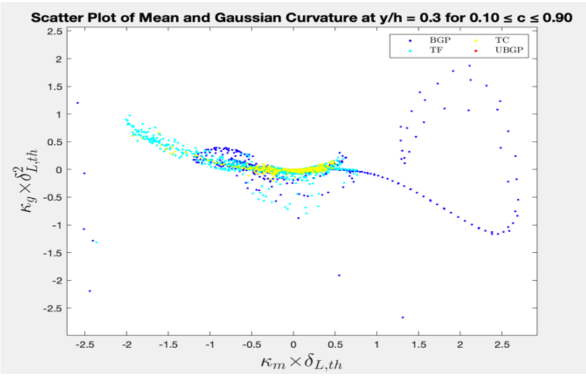

Figure 11 (c.iii)

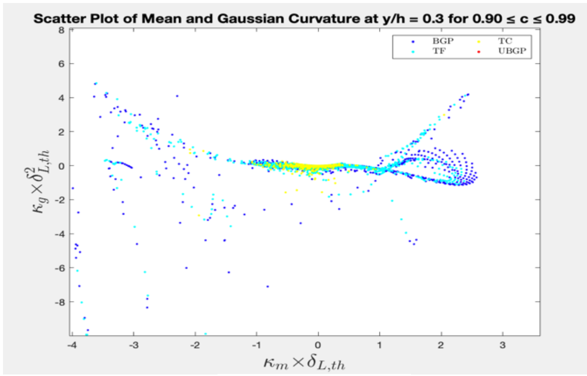

Figure 11 (c.iv)

4.6.4. Mean and Gaussian Curvatures at y/h = 0.6

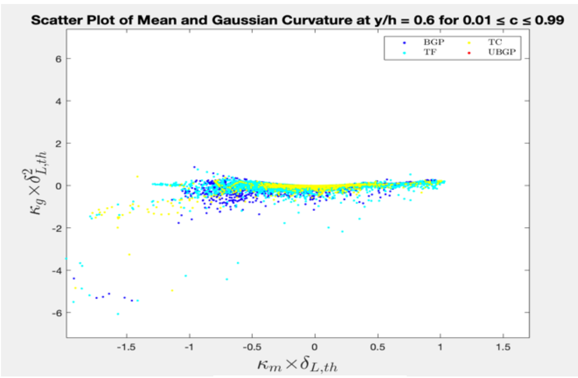

Figure 11 (d.i)

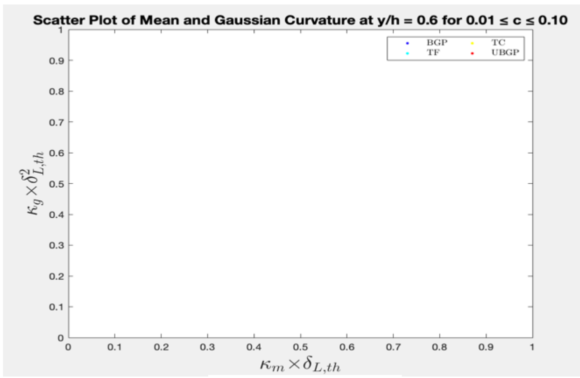

Figure 11 (d.ii)

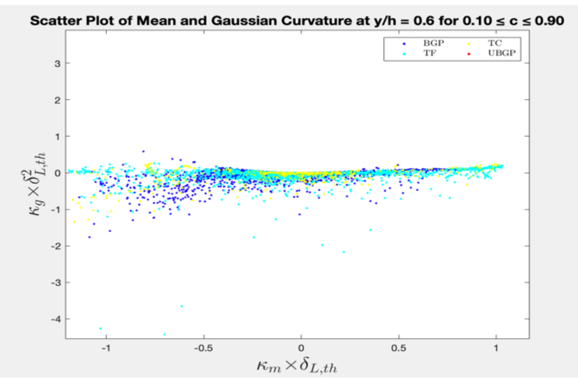

Figure 11 (d.iii)

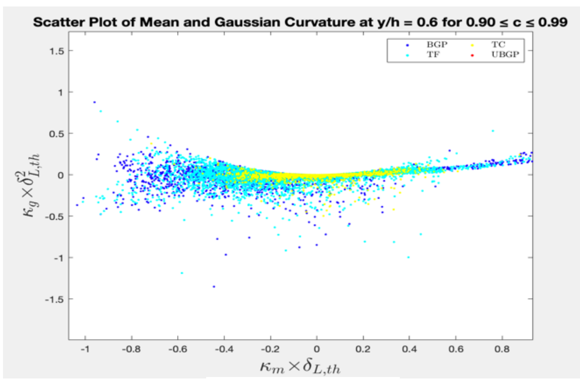

Figure 11 (d.iv)

4.6.5. Mean and Gaussian Curvatures y/h = 0.95

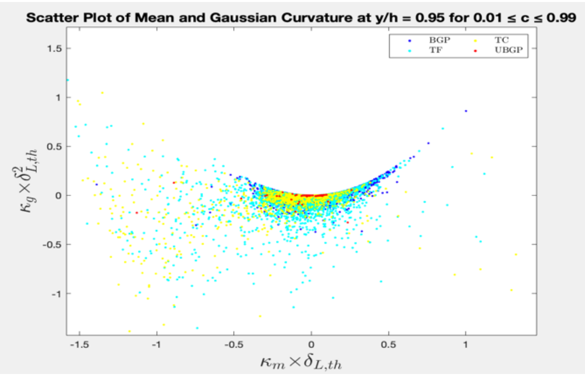

Figure 11 (e.i)

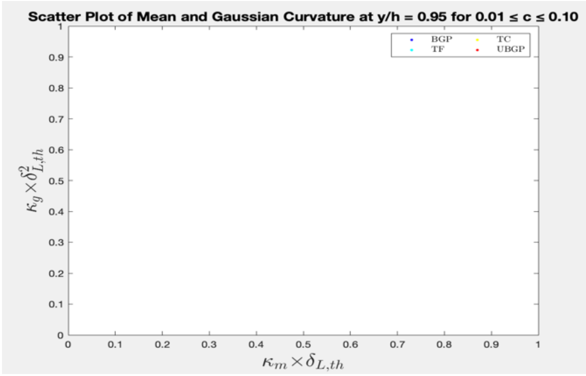

Figure 11 (e.ii)

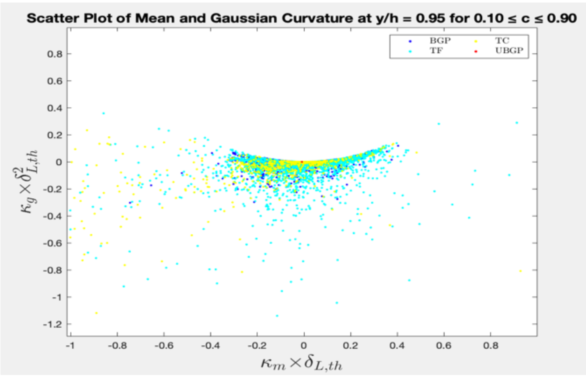

Figure 11 (e.iii)

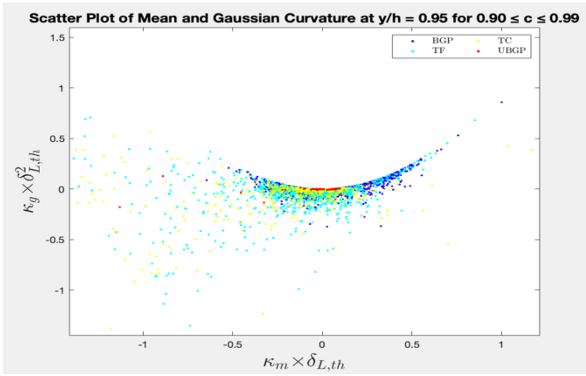

Figure 11 (e.iv)

4.6.6. Mean and Gaussian Curvatures y/h = 1

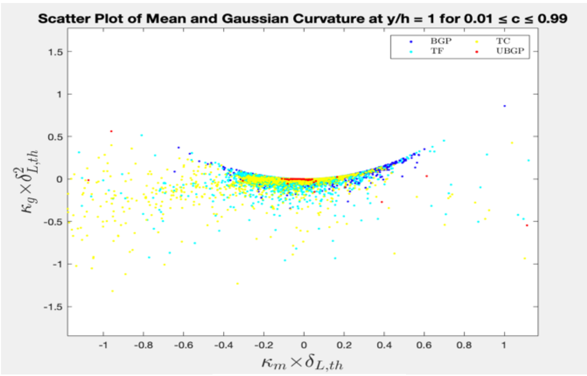

Figure 11 (f.i)

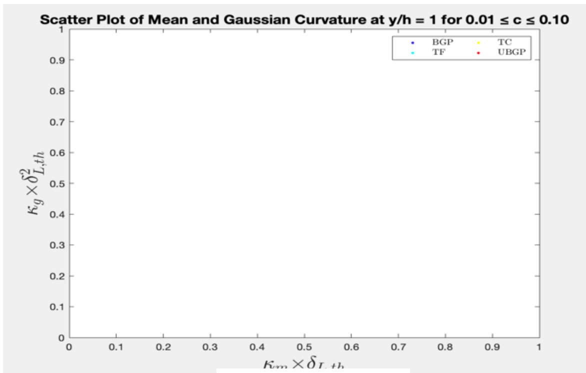

Figure 11 (f.ii)

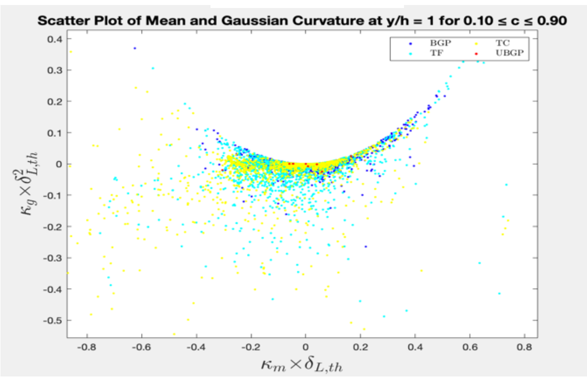

Figure 11 (f.iii)

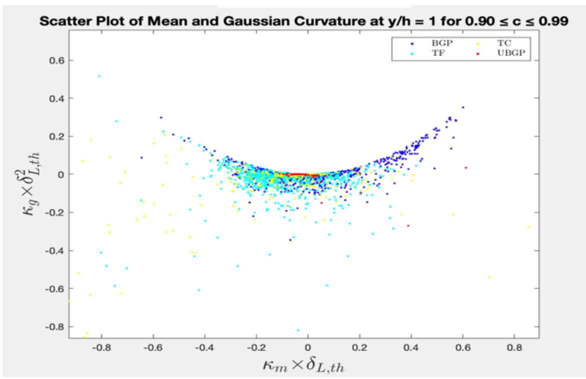

Figure 11 (f.iv)

Figure 10. Scatter of $\kappa_g \times \delta_{L,th}^2$ *with* $\kappa_m \times \delta_{L,th}$ for the FSI events at (a) *y/h* = 0.05, (b) *y/h* = 0.1, (c) *y/h* = 0.3, (d) *y/h* = 0.6, (e) *y/h* = 0.95, (f) *y/h* =1 for (i) 0.01 $\leq c \leq$ 0.99, (ii) 0.01 $\leq c \leq$ 0.10, (iii) 0.10 $\leq c \leq$ 0.90, (iv) 0.90 $\leq c \leq$ 0.99, The scatter colour is based upon the different FSI topology: Red = UBGP, Cyan = TF, Yellow = TC, Blue = BGP

4.6.7. Mean and Gaussian Curvatures Discussion

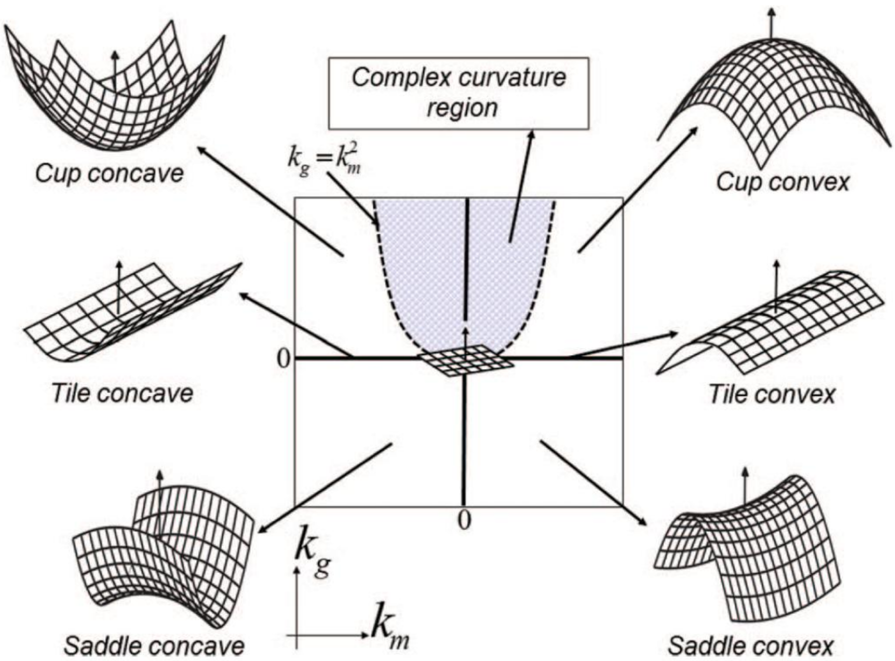

Figure 12. Classification of iso-scalar surface geometries in terms of their mean and gaussian curvatures, κ_m & κ_g[56]

The local geometries of the flame surface can be characterised based on the local mean curvature $\kappa_m = 0.5\nabla \cdot (-\nabla c/|\nabla c|) = (\kappa_1 + \kappa_2)/2$ and the Gaussian curvature $\kappa_g = \kappa_1 \times \kappa_2$,[52,57,58] where κ_1 and κ_2 are the two principal curvatures. Note the region of $\kappa_g > \kappa_m^2$ shows as the shaded region in figure 12 is not realisable because it leads to complex principal curvatures.

Condition	Topology Description
$\kappa_g > 0$	Elliptical Cup-Like Type
$\kappa_g < 0$	Hyperbolic Saddle
$\kappa_m > 0$	Convex to Unburned Reactants
$\kappa_m < 0$	Concave to Unburned Reactants
$\kappa_g = 0 \; and \; \kappa_m > 0$	Tile-Like Convex
$\kappa_g = 0 \; and \; \kappa_m < 0$	Tile-Like Concave
$\kappa_g = 0 \; and \; \kappa_m = 0$	Flat

Table 5. Conditions of mean and Gaussian curvatures κ_m & κ_g required to produce corresponding geometrical iso-scalar surfaces of the flame surface.

Figure 11 shows the scatter plots of the four different topologies (UBGP, BGP, TC, TF) for $0.01 \leq c \leq 0.99$, $0.01 \leq c \leq 0.10$, $0.10 \leq c \leq 0.90$ and $0.90 \leq c \leq 0.99$ at all axial positions analysed within this study made dimensionless using the laminar flame thickness $\delta_{L,th}$. Table 5 outlines the surface geometry of a flame element for different values of mean and Gaussian curvatures. Analysing figure 12 and applying the conditions outlined in table 5, the geometrical surfaces of the FSI events can be described for a hydrogen-rich flame undergoing boundary layer flashback by using the mean and Gaussian curvatures.

The first thing observable from figure 11 is the absence FSI events at $0.01 \leq c \leq 0.10$ at all wall normal distances within the channel flow which is in agreement with figures 9 and 10. This suggests the flame only collides and interacts with itself towards the hot products region of the domain or the trailing edge of the flame brush.

y/h Value	FSI Topology	Predominant Surface Type(s)
0.05	BGP	Cup Convex
	TF	Cup Convex
	TC	Cup Convex
	UBGP	-
0.1	BGP	Cup Convex or Saddle Convex
	TF	Cup Convex or Saddle Convex
	TC	Cup Convex
	UBGP	-
0.3	BGP	Cup Convex or Saddle Convex
	TF	Cup Concave or Cup Convex
	TC	Cup Concave
	UBGP	-
0.6	BGP	Cup Concave or Saddle Concave
	TF	Cup Concave or Cup Convex or Saddle Concave
	TC	Saddle Convex or Saddle Concave
	UBGP	-
0.95	BGP	Cup Convex or Saddle Convex
	TF	Saddle Convex or Saddle Concave
	TC	Saddle Concave
	UBGP	Saddle Convex or Saddle Concave
1.0	BGP	Cup Convex
	TF	Saddle Concave
	TC	Saddle Convex or Saddle Concave
	UBGP	Saddle Concave

Table 6. Predominant iso-scalar surface geometries for each FSI topology type at all wall normal distances analysed in this study based of the mean and Gaussian curvatures, κ_m & κ_g from figures 11.

Table 6 outlines the iso-scalar surface geometries which are most predominantly associated to describe the four different FSI topology types at all wall normal distances analysed in this study. From table 6 it is evident that all the FSI events within the vicinity of the boundary layer (y/h = 0.05 and y/h = 0.1) are geometrically described to have a convex surface type towards the unburned reactants, in either a cup shape or less frequently a saddle shape. The type of surface geometry attached to each FSI topology varies greatly as progression is made away from the wall boundary s.

In the region at the middle of the channel flow, the TC, TF and UBGP FSI geometries tend to become saddle shaped whilst the BGP's stayed cup-like. The cup convex surface geometry is the most frequent geometry with eleven instances of being the most predominant, followed by the saddle concave holding nine instances, then the saddle convex next holding eight instances, and finally the cup concave surface type being the rarest with four instances of description. Furthermore, it can be seen from table 6 that BGP's are most commonly described to have a cup convex surface type, and the UBGP's to most commonly have a saddle concave geometry. The surface geometries of the TF and TC FSI topologies can be seen from table 6 to most frequently be described by cup convex and saddle concave surface types respectfully.

It should be noted that the aforementioned predominant surface geometries observed to be associated with the FSI topologies in this study of boundary layer flashback are inconsistent with two earlier studies. A FSI study of spherically expanding flames propagating into fuel droplet-mists[52] and an FSI study of an open turbulent jet spray flame[16] mutually describe the surface geometries of UBGPs, BGPs, TFs and TCs to be concave cup-like, convex cup-like, hyperbolic saddle and hyperbolic saddle respectively. This discrepancy for the UBGP and the TF topologies could be a result of the physical differences the turbulent boundary layer introduces to the fluid flow when comparing it to a freely propagating flame as simulated in the previous studies. Another more probable explanation suggests there could be an error within this study on the calculation of the mean and Gaussian curvatures and further work would need to be carried out in the future to validate this.

5. Conclusion

A Direct Numerical Simulation (DNS) database of a premixed hydrogen-air flame in turbulent boundary layer flashback has been analysed to investigate the Flame Self-Interactions (FSIs) in fully developed shear generated turbulence for the first time. The occurrences of the FSIs [i.e., Burned Gas Pockets (BGP), Unburned Gas Pockets (UBGP), Tunnel Closures (TC), Tunnel Formation (TF)] have been analysed across the channel flow at different differences from the wall boundary . It has been found that the presence of the wall boundary has a significant influence on the geometry of the flames surface and consequently the overall turbulent burning rate. At all wall normal distances , it was found that the FSI events were located within a very confined region of the trailing edge of the flame brush towards the hot burnt products. Inconsistent with other analyses, BGPs occurred more frequently than TCs, and UBGPs only existed towards the middle of the channel flow where the flow velocity was at a maximum ($y/h \approx 1$). The latter was explained due to the transient nature of such an event and with flame pinch-off being more frequent at maximum flow velocity. The back-to-back TC events lead to the formation of an UBGP which causes flame pinch-off. This rapidly effected the flames surface area and consequently the overall turbulent burning rate. The head-on TF events lead to the formation of a BGP. Understanding the statistical behaviours of these FSI events and most importantly their frequency of occurrence is of fundamental importance to formulate more accurate models of turbulent premixed hydrogen-rich combustion in boundary layer flashback. The results presented in this study have important implications from a modelling perspective where the flame topologies have a strong influence on the geometry of the flames surface, which will inevitably affect and possibly provide an extension to the flame surface-based modelling approaches. Accordingly, the findings of the current analysis might need to be considered when extending such flame surfaced-based models in the context of turbulent premixed flames at boundary layer flashback, perhaps used in the design of modern industrial combustion equipment.

6. References

(1) O. Bolland and H. Undrum, "A novel methodology for comparing CO2 capture options for natural gas-fired combined cycle plants," Adv. Environ. Res. 7(4), 901– 911 (2003).
(2) T. C. Lieuwen, V. McDonell, E. Petersen, and D. Santavicca, "Fuel flexibility influences on premixed combustor blowout, flashback, autoignition, and stability," J. Eng. Gas Turbines Power 130(1), 011506 (2008).
(3) U. Ahmed, A. Pillai, N. Chakraborty and R. Kurose, "Statistical behavior of turbulent kinetic energy transport in boundary layer flashback of hydrogen-rich premixed combustion", *Physical Review Fluids*, vol. 4, no. 10, 2019.
(4) C. Mayer, J. Sangl, T. Sattelmayer, T. Lachaux, and S. Bernero. Study on the Operational Window of a Swirl Stabilized Syngas Burner Under Atmospheric and High-Pressure Conditions. J. Eng. Gas Turbines Power, 134(3):031506, 2012.
(5) A. Gruber, J. H. Chen, D. Valiev, and C. K. Law. Direct numerical simulation of premixed flame boundary layer flashback in turbulent channel flow. J. Fluid Mech., 709:516-542, 2012.
(6) U. Ahmed, N. A. K. Doan, J. Lai, M. Klein, N. Chakraborty, and N. Swaminathan, "Multiscale analysis of head-on quenching premixed turbulent flames," Phys. Fluids 30(10), 105102 (2018).
(7) O. J. Ugarte, V. Bychkov, J. Sadek, D. Valiev, and V. y. Akkerman, "Critical role of blockage ratio for flame acceleration in channels with tightly spaced obstacles," Phys. Fluids 28(9), 093602 (2016). Phys. Fluids 28(9), 093602 (2016).
(8) M. Boger, D. Veynante, H. Boughanem, and A. Trouv., "Direct numerical simulation analysis of flame surface density concept for large eddy simulation of turbulent premixed combustion," Proc. Combust. Inst. 27(1), 917–925 (1998).
(9) R. Borghi and D. Dutoya, "On the scales of the fluctuations in turbulent combustion," Symp. (Int.) Combust. 17(1), 235–244 (1979).
(10) W. Kollmann and J. H. Chen, "Pocket formation and the flame surface density equation," Proc. Combust. Inst. 27(1), 927–934 (1998).
(11) FRITZ, J., KR¨O NER, M. & SATTELMAYER, T. 2004 Flashback in a swirl burner with cylindrical premixing zone. ASME J. Engine Gas Turbines Power 126, 276–283.
(12) R. S. Cant, C. J. Rutland, and A. Trouve, "Statistics for laminar flamelet modelling," in Proceeding of the Summer Program 1990, Center for Turbulence Research, Stanford (1990), pp. 271–279.
(13) K. W. Jenkins and R. S. Cant, "Curvature effects on flame kernels in a turbulent environment," Proc. Combust. Inst. 29, 2023–2029 (2002).
(14) N. Chakraborty and R. S. Cant, "Statistical behaviour and modelling of flame normal vector in turbulent premixed flames," Numer. Heat Transfer, Part A 50, 623–643 (2006).
(15) T. D. Dunstan and N. Swaminathan, "Flame interactions in turbulent premixed twin V-flames," Combust. Sci. Technol. 185, 134–159 (2013).
(16) S. Malkeson, U. Ahmed, A. Pillai, N. Chakraborty and R. Kurose, "Flame self-interactions in an open turbulent jet spray flame", *Physics of Fluids*, vol. 33, no. 3, p. 035114, 2021.
(17) R. A. C. Griffiths, J. H. Chen, H. Kolla, R. S. Cant, and W. Kollmann, "Three dimensional topology of turbulent premixed flame interaction," Proc. Combust. Inst. 35, 1341–1348 (2015).
(18) R. Y. Minamoto, B. Yenerdag, and M. Tanahashi, "Morphology and structure of hydrogen-air turbulent premixed flames," Combust. Flame 192, 369–383 (2018).
(19) A. K. Doan, N. Swaminathan, and Y. Minamoto, "DNS of MILD combustion with mixture fraction variations," Combust. Flame 189, 173–189 (2018).
(20) S. Trivedi, G. V. Nivarti, and R. S. Cant, "Flame self-interactions with increasing turbulence intensity," Proc. Combust. Inst. 37, 2443–2449 (2019).
(21) S. Trivedi, R. A. C. Griffiths, J. H. Chen, H. Kolla, and R. S. Cant, "Topology of pocket formation in turbulent premixed flames," Proc. Combust. Inst. 37, 2619–2626 (2019).
(22) A. Tyagi, I. Boxx, S. Peluso, and J. O'Connor, "The role of flow interaction in flame–flame interaction events in a dual burner experiment," Proc. Combust. Inst. 37, 2485–2491 (2019).
(23) F. Ladeinde, E. E. O'Brien, W. Liu, and X. D. Cai, "Fundamental studies of three dimensional, chemically-reacting compressible turbulence," in International Colloquium on Advanced Computation & Analysis of Combustion, Moscow, Russia (1997).

(24) F. Ladeinde, W. Liu, and E. E. O'Brien, "DNS studies of turbulence in compressible mixing layers," in ASME Fluid Engineering Conference, Vancouver, Canada (1997).
(25) X. Cai, F. Ladeinde, and E. E. O'Brien, "Parallel DNS with MPI in SP/2," in First Air Force Office of Scientific Research (AFOSR) Conference on DNS and LES, Louisiana, USA (1997).
(26) F. Ladeinde, W. Liu, and E. E. O'Brien, "DNS evaluation of chemistry models for compressible non-premixed flames," in AIAA (1999).
(27) T. Kitano, T. Tsuji, R. Kurose, and S. Komori, "Effect of pressure oscillations on flashback characteristics in a turbulent channel flow," Energy Fuels 29(10), 6815– 6822 (2015).
(28) A. L. Pillai and R. Kurose, "Combustion noise analysis of a turbulent spray flame using a hybrid DNS/APE-RF approach," Combust. Flame 200, 168–191 (2019). (29) Y. Hu and R. Kurose, "Nonpremixed and premixed flamelets LES of partially premixed spray flames using a two-phase transport equation of progress variable," Combust. Flame 188, 227–242 (2018).
(30) U. Ahmed, C. Turquand d'Auzay, M. Muto, N. Chakraborty, and R. Kurose, "Statistics of reaction progress variable and mixture fraction gradients of a pulverised coal jet flame using direct numerical simulation data," Proc. Combust. Inst. 37(3), 2821–2830 (2019).
(31) T. Hara, M. Muto, T. Kitano, R. Kurose, and S. Komori, "Direct numerical simulation of a pulverized coal jet flame employing a global volatile matter reaction scheme based on detailed reaction mechanism," Combust. Flame 162(12), 4391–4407 (2015).
(32) C. Turquand d'Auzay, U. Ahmed, A. L. Pillai, N. Chakraborty, and R. Kurose, "Statistics of progress variable and mixture fraction gradients in an open turbulent jet spray flame," Fuel 247, 198–208 (2019).
(33) J. A. Miller and C. T. Bowman, "Mechanism and modeling of nitrogen chemistry in combustion," Prog. Energy Combust. Sci. 15(4), 287 338 (1989).
(34) B. P. Leonard, "A stable and accurate convective modelling procedure based on quadratic upstream interpolation," Comput. Methods Appl. Mech. Eng. 19(1), 59–98 (1979).
(35) J. Lee, S. Yoon Jung, H. Jin Sung, and T. A. Zaki, "Effect of wall heating on turbulent boundary layers with temperature-dependent viscosity," J. Fluid Mech. 726, 196–225 (2013).
(36) H. Abe, H. Kawamura, and Y. Matsuo, "Surface heat-flux fluctuations in a turbulent channel flow up to $Re\tau = 1020$ with $Pr = 0.025$ and 0.71," Int. J. Heat Fluid Flow 25(3), 404–419 (2004).
(37) V. Moureau, C. B.rat, and H. Pitsch, "An efficient semi-implicit compressible solver for large-eddy simulations," J. Comput. Phys. 226(2), 1256 1270 (2007).
(2007).
(38) F. A. Williams, Combustion Theory, 2nd ed. (CRC Press, 1994).
(39)A. Ern and V. Giovangigli, Multicomponent Transport Algorithms (Springer Verlag, Heidelberg, 1994).
(40) R. Kee, F. Rupley, and J. Miller, "Chemkin-II, A FORTRAN chemical kinetics package for the analysis of gas-phase chemical kinetics," Technical report, Sandia National Laboratories, Albuquerque, NM, Livermore, CA, 1989.
(41) Surface density function evolution and the influence of strain rates during turbulent boundary layer flashback of hydrogen-rich premixed combustion.
(42) T. J. Poinsot and S. K. Lelef, "Boundary conditions for direct simulations of compressible viscous flows," J. Comput. Phys. 101(1), 104–129 (1992).
(43) H. Pitsch, A C ++ Computer Program for 0D Combustion and 1D Laminar Flame Calculations,
(44) R. D. Moser, J. Kim, and N. N. Mansour, "Direct numerical simulation of turbulent channel flow up to $Re\tau=590$," Phys. Fluids 11(4), 943–945 (1999).
(45) N. Chakraborty, "Comparison of displacement speed statistics of turbulent premixed flames in the regimes representing combustion in corrugated flamelets and thin reaction zones," Phys. Fluids 19(10), 105109 (2007).
(46) R. Sankaran, E. R. Hawkes, J. H. Chen, T. Lu, and C. K. Law, "Structure of a spatially developing turbulent lean methane-air Bunsen flame," Proc. Combust. Inst. 31(1), 1291–1298 (2007).
(47) H. Wang, E. R. Hawkes, J. H. Chen, B. Zhou, Z. Li, and M. Ald.n, "Direct numerical simulations of a high Karlovitz number laboratory premixed jet flame— An analysis of flame stretch and flame thickening," J. Fluid Mech. 815, 511–536 (2017).

(48) A. Sandeep, F. Proch, A. M. Kempf, and N. Chakraborty, "Statistics of strain rates and surface density function in a flame-resolved high-fidelity simulation of a turbulent premixed bluff body burner," Phys. Fluids 30(6), 065101 (2018).
(49)R. Griffiths, J. Chen, H. Kolla, R. Cant and W. Kollmann, "Three-dimensional topology of turbulent premixed flame interaction", *Proceedings of the Combustion Institute*, vol. 35, no. 2, pp. 1341-1348, 2015. Available: 10.1016/j.proci.2014.08.003.
(50) N. Chakraborty and R. S. Cant, "Influence of Lewis number on curvature effects in turbulent premixed flame propagation in the thin reaction zones regime," Phys. Fluids 17(10), 105105 (2005).
(51) S. H. Kim and H. Pitsch, "Scalar gradient and small-scale structure in turbulent premixed combustion," Phys. Fluids 19(11), 115104 (2007).
(52) G. Ozel-Erol, U. Ahmed, and N. Chakraborty, "Flame self-interactions in globally stoichiometric spherically expanding flames propagating into fuel droplet-mists," Proc. Combust. Inst. (published online, 2020).
(53) S. Chaudhuri, H. Kolla, E.R. Hawkes, J.H. Chen, C.K. Law, J. Fluid Mech. (2013)
(54) Flame Thickness and Conditional Scalar Dissipation Rate in a Premixed Temporal Turbulent Reacting Jet
(55) J.H. Chen, T. Echekki, W. Kollmann, Combust. Flame 116 (1999) 15–48.
(56)L. Cifuentes, C. Dopazo, J. Martin and C. Jimenez, "Local flow topologies and scalar structures in a turbulent premixed flame", *Physics of Fluids*, vol. 26, no. 6, p. 065108, 2014. Available: 10.1063/1.4884555.
(57) C. Dopazo , J. Martin , J. Hierro , *Phys.Rev..E*76 (2007) 056316 .
(58) R.S. Cant , C.J. Rutland , A. Trouvé, in: Proceeding of the Summer Program 1990, Center for Turbulence
(59) T. D. Dunstan, N. Swaminathan, K. N. C. Bray, and N. Kingsbury, "The effects of non-unity Lewis numbers on turbulent premixed flame interactions in a twin V-flame configuration," Combust. Sci. Technol. 185, 874–897 (2013).
(60) Z. Sun, "Structure of turbulent rich hydrogen-air premixed flames", *International Journal of Energy Research*, vol. 42, no. 8, pp. 2845-2858, 2018. Available: 10.1002/er.4048.
(61) Sun ZY, Li GX. On reliability and flexibility of sustainable energy application route for vehicles in China. *Renew Sustain Energy Rev*. 2015; **51:830**-846.

NOTE TO SELF

The gaussian curvature of the scalar field within the DNS domain can be described to second order by a quadratic function. The coefficients of this quadratic correspond to the eigenvalues which are parameterised to + or – Unity. These new eigenvalues then determine the FSI topologies associated with that local geometry of the scalar field within the computational domain.